



HAL
open science

Mutant SOD1 and mitochondrial damage alter expression and splicing of genes controlling neuritogenesis in models of neurodegeneration

Silvia Carolina Lenzken, Valentina Romeo, Francesca Zolezzi, Francesca Cordero, Giuseppe Lamorte, Davide Bonanno, Donatella Biancolini, Mauro Cozzolino, Maria Grazia Pesaresi, Alessia Maracchioni, et al.

► To cite this version:

Silvia Carolina Lenzken, Valentina Romeo, Francesca Zolezzi, Francesca Cordero, Giuseppe Lamorte, et al.. Mutant SOD1 and mitochondrial damage alter expression and splicing of genes controlling neuritogenesis in models of neurodegeneration. *Human Mutation*, 2011, 32 (2), pp.168. 10.1002/humu.21394 . hal-00610796

HAL Id: hal-00610796

<https://hal.science/hal-00610796>

Submitted on 25 Jul 2011

HAL is a multi-disciplinary open access archive for the deposit and dissemination of scientific research documents, whether they are published or not. The documents may come from teaching and research institutions in France or abroad, or from public or private research centers.

L'archive ouverte pluridisciplinaire **HAL**, est destinée au dépôt et à la diffusion de documents scientifiques de niveau recherche, publiés ou non, émanant des établissements d'enseignement et de recherche français ou étrangers, des laboratoires publics ou privés.



Mutant SOD1 and mitochondrial damage alter expression and splicing of genes controlling neuritogenesis in models of neurodegeneration

Journal:	<i>Human Mutation</i>
Manuscript ID:	humu-2010-0331.R1
Wiley - Manuscript type:	Research Article
Date Submitted by the Author:	15-Sep-2010
Complete List of Authors:	<p>Lenzken, Silvia; University of Milano-Bicocca, Department of Biotechnology and Biosciences Romeo, Valentina; University of Milano-Bicocca, Department of Biotechnology and Biosciences Zolezzi, Francesca; Genopolis Consortium, University of Milano-Bicocca, Department of Biotechnology and Biosciences Cordero, Francesca; University of Torino, Department of Clinical and Biological Sciences Lamorte, Giuseppe; University of Milano-Bicocca, Department of Biotechnology and Biosciences Bonanno, Davide; University of Milano-Bicocca, Department of Biotechnology and Biosciences Biancolini, Donatella; Genopolis Consortium, University of Milano-Bicocca, Department of Biotechnology and Biosciences Cozzolino, Mauro; Fondazione Santa Lucia, IRCCS Pesaresi, Maria; Fondazione Santa Lucia, IRCCS; University of Rome "Tor Vergata, Department of Biology Maracchioni, Alessia; Fondazione Santa Lucia, IRCCS Sanges, Remo; CBM scl - Genomics Achsel, Tilmann; Katholieke Universiteit, VIB, Department of Molecular and Developmental Genetics; Fondazione Santa Lucia, IRCCS Carrì, Maria; University of Rome "Tor Vergata, Department of Biology; Fondazione Santa Lucia, IRCCS Calogero, Raffaele; University of Torino, Department of Clinical and Biological Sciences Barabino, Silvia; Università di Milano-Bicocca, Biotechnology and Biosciences</p>
Key Words:	ALS, axon guidance, microarray, mitochondria, neurodegeneration, RNA splicing, SOD1

1
2
3
4
5
6
7
8
9
10
11
12
13
14
15
16
17
18
19
20
21
22
23
24
25
26
27
28
29
30
31
32
33
34
35
36
37
38
39
40
41
42
43
44
45
46
47
48
49
50
51
52
53
54
55
56
57
58
59
60

SCHOLARONE™
Manuscripts

For Peer Review

1
2
3 **Mutant SOD1 and mitochondrial damage alter expression and splicing of genes**
4 **controlling neuritogenesis in models of neurodegeneration**
5
6
7

8 Silvia C. Lenzken¹, Valentina Romeo¹, Francesca Zolezzi², Francesca Cordero³,
9
10 Giuseppe Lamorte¹, Davide Bonanno¹, Donatella Biancolini², Mauro Cozzolino⁶,
11
12 Maria Grazia Pesaresi⁶, Alessia Maracchioni⁶, Remo Sanges⁷, Tilmann Achsel^{4,6},
13
14 Maria Teresa Carri^{5,6}, Raffaele A. Calogero³, and Silvia M.L. Barabino^{1*}
15
16

17
18 ¹Department of Biotechnology and Biosciences, University of Milano-Bicocca, Piazza
19 della Scienza, 2, 20126 Milano, Italy
20

21
22 ² Genopolis Consortium, University of Milano-Bicocca, Piazza della Scienza 2-4,
23 20126 Milano, Italy
24

25
26 ³ Department of Clinical and Biological Sciences, University of Torino, Regione
27 Gonzole 10, Orbassano, 10043, Torino, Italy
28

29
30 ⁴ VIB Department of Molecular and Developmental Genetics, KU Leuven, Belgium
31

32
33 ⁵ Department of Biology, University of Rome "Tor Vergata," Rome, Italy.
34

35
36 ⁶ Laboratory of Neurochemistry, Fondazione Santa Lucia, IRCCS, Rome, Italy.
37

38
39 ⁷ CBM srl - Genomics, Area Science Park, Basovizza, Trieste, Italy
40
41

42
43 Running title: Alternative splicing and neurodegeneration
44

45
46 Keywords: ALS, axon guidance, microarray, mitochondria, neurodegeneration, RNA
47 splicing, SOD1
48
49

50
51 *Corresponding author: Silvia M.L. Barabino
52
53
54

1
2
3
4
5
6
7
8
9
10
11
12
13
14
15
16
17
18
19
20
21
22
23
24
25
26
27
28
29
30
31
32
33
34
35
36
37
38
39
40
41
42
43
44
45
46
47
48
49
50
51
52
53
54
55
56
57
58
59
60

Department of Biotechnology and Biosciences
University of Milano-Bicocca, Piazza della Scienza, 2
I-20126 Milano, Italy;
Phone: +39-02-6448 3352
Fax: +39-02-6448 3569
E-mail: silvia.barabino@unimib.it

For Peer Review

Abstract

Mitochondrial dysfunction has been implicated in the pathogenesis of a number of neurodegenerative disorders including Parkinson, Alzheimer and Amyotrophic Lateral Sclerosis (ALS). In addition, aberrant mRNA splicing has been documented in neurodegeneration. To characterize the cellular response to mitochondrial perturbations at the level of gene expression and alternative pre-mRNA splicing we used splicing-sensitive microarrays to profile human neuroblastoma SH-SY5Y cells treated with paraquat, a neurotoxic herbicide that induces the formation of reactive oxygen species and causes mitochondrial damage in animal models, and SH-SY5Y cells stably expressing the mutant G93A-SOD1 protein, one of the genetic causes of ALS. In both models we identified a common set of genes whose expression and alternative splicing are deregulated. Pathway analysis of the deregulated genes revealed enrichment in genes involved in neuritogenesis, axon growth and guidance, and synaptogenesis. Alterations in transcription and pre-mRNA splicing of candidate genes were confirmed experimentally in the cell line models as well as in brain and spinal cord of transgenic mice carrying the G93A-SOD1 mutation. Our findings expand the realm of the pathways implicated in neurodegeneration and suggest that alterations of axonal function may descend directly from mitochondrial damage.

Deleted: 's disease

Deleted: 's disease

Introduction

Mitochondrial dysfunction has been directly or indirectly implicated in the pathogenesis of a number of neurodegenerative disorders including Parkinson, Alzheimer, and Huntington (Gibson, et al., 2009). In recent years, mitochondrial damage has also emerged as an early factor contributing to the pathogenesis of Amyotrophic Lateral Sclerosis (ALS, Magrane and Manfredi, 2009).

ALS is a progressive, invariably fatal, neurodegenerative disease caused by the degeneration of motor neurons (Boillee, et al., 2006). Sporadic ALS (sALS) is a genetically and clinically very heterogeneous disease (Chio, et al., 2009). The aetiology of sALS is largely unknown but is likely linked to both environmental and genetic factors inducing mechanisms of motor neuron damage. These mechanisms include oxidative damage, accumulation of intracellular aggregates, mitochondrial failure, defects in axonal transport, growth factor deficiency, aberrant RNA metabolism, glial cell pathology, and glutamate excitotoxicity (Cozzolino, et al., 2008; Rothstein, 2009). Familial ALS (fALS) accounts for approximately 5%–10% of all ALS cases and is caused by genetic factors. Of these, approximately 1 in 5 are linked to a mutation in copper/zinc superoxide dismutase 1 (*SOD1*, #MIM 147450), an enzyme responsible for scavenging the free O_2^- radicals.

There is a substantial body of evidence indicating that mitochondrial dysfunction is a feature of motor neuron degeneration in ALS. Mitochondrial damage has been reported both in sporadic and familial ALS patients and in cellular and animal models that express mutant *SOD1* (Shi, et al., 2010). Mitochondrial dysfunction may lead to the degeneration of motor neurons because of energy deprivation following impairment of the respiratory chain, alteration of intracellular calcium handling and activation of the apoptotic pathway. We have recently reported that mitochondrial

Deleted: 's Disease

Deleted: 's Disease

1
2
3 dysfunction caused by paraquat (N,N'-dimethyl-4,4'-bipyridinium dichloride, PQ), a
4 neurotoxic herbicide that induces Parkinsonian features in animal models, has
5 another, quite unexpected effect, i.e. it modulates alternative splicing of a set of
6 mRNAs in cells of neuronal origin (Maracchioni, et al., 2007). The importance of
7 alternative splicing (AS) in regulating gene expression is illustrated by a growing
8 number of diseases associated with abnormal mRNA patterns (for review see
9 (Cooper, et al., 2009). Alterations of the splicing pattern of several mRNAs have been
10 reported in ALS patients and in murine models (Aerbajinai, et al., 2002; Munch, et al.,
11 2002; Pantelidou, et al., 2007; Robertson, et al., 2003; Tomiyama, et al., 2002).
12 Recently, the identification in fALS patients of mutations in *TARDBP* (MIM#
13 605068) and *FUS* (MIM# 13070) that encode DNA/RNA-binding proteins has further
14 strengthened the idea that splicing abnormalities may contribute to neurodegeneration
15 (Lagier-Tourenne and Cleveland, 2009).
16
17

18
19 Based on these reports, we hypothesized that not only gene expression but also
20 alternative pre-mRNA splicing might be altered in neurodegenerative conditions
21 involving mitochondrial damage such as ALS, or Parkinson's disease. We thus
22 performed a whole-genome, exon level analysis of the cellular response to
23 mitochondrial failure. Using Affimetrix Exon 1.0 ST GeneChips® microarrays we
24 profiled human neuroblastoma SH-SY5Y cells treated with PQ, and SH-SY5Y cells
25 stably expressing the mutant G93A-SOD1protein, which is one of the genetic causes
26 of ALS. We then combined the data sets from the two experiments to identify
27 common molecular pathways underlying the response to mitochondrial insufficiency.
28
29 The results revealed alterations in the transcriptional and post-transcriptional
30 expression of several genes involved in neuritogenesis and support a role for the
31
32
33
34
35
36
37
38
39
40
41
42
43
44
45
46
47
48
49
50
51
52
53
54
55
56
57
58
59
60

1
2 alteration in axon growth and guidance molecules as a partner in mitochondria-
3 mediated neurodegeneration.
4
5

6 7 8 **Materials and Methods** 9

10 *Cell culture*

11
12 Human neuroblastoma SH-SY5Y untransfected or stably transfected with cDNAs
13 coding for wild type SOD1 or the mutant G93A-SOD1 (Carri, et al., 1997), were
14 cultured in D-MEM/F-12 media with GlutaMAX™ (Gibco, Invitrogen, UK), 10%
15 FBS, 100 Units/ml penicillin G, 100µg/ml streptomycin/ penicillin (Euroclone,
16 Milano, Italy). Stably transfected cells were also maintained in the presence of
17 400µg/ml Geneticin (G418 sulphate, Euroclone). Cells were fed every 2–3 days and
18 passed once a week. For the microarray experiment, after an initial amplification of
19 each cell type, cells were aliquoted and stored in liquid nitrogen. For every
20 experiment an aliquot of each cell line was thawed and seeded. After having reached
21 confluence, cells were reseeded at 3×10^6 cells in 100mm dish. Paraquat (N,N'-
22 dimethyl-4,4'-bipyridinium dichloride, Sigma-Aldrich) treatment was carried out
23 essentially as described in (Maracchioni, et al., 2007) but for 18 h at 0,75 mM
24 concentration.
25
26
27
28
29
30
31
32
33
34
35
36
37
38
39
40

41 *RNA preparation*

42
43 Total RNA was from cultured cells extracted using TRIzol® Reagent (Invitrogen),
44 and subsequently purified using silica membrane spin columns from RNeasy Mini kit
45 (Qiagen). RNA quantity and purity were assessed using a NanoDrop® instrument
46 (Thermo Fisher Scientific Inc.). Total RNA integrity was assessed by using a 2100
47 Bioanalyzer (Agilent Technologies) and the RNA Integrity Number (RIN) was
48
49
50
51
52
53
54
55
56
57
58
59
60

1
2 calculated. Mouse total RNA was isolated from brain and spinal cord with TRIzol®
3
4 Reagent (Invitrogen) from eleven healthy female mice (controls) and fourteen female
5
6 G93A-SOD1 mice sacrificed between 93 and 170 days.
7
8
9

10 *Microarray hybridization and data analysis*

11
12 Each condition was replicated 5 times. After extraction and quality check 1.5 µg of
13
14 total RNA was subjected to removal of ribosomal RNA following the procedure
15
16 suggested by the manufacturer (Affymetrix). The resulting total RNA was then used
17
18 to create the biotin-labelled library to be hybridized on GeneChip® Exon 1.0 ST
19
20 human microarrays following the procedure described by the manufacturer
21
22 (Affymetrix). The CEL files resulting from the hybridization were analyzed using
23
24 oneChannelGUI 1.6.5 (Sanges, et al., 2007). Gene-level calculation was performed by
25
26 RMA (Robust Multichip Average, (Irizarry, et al., 2003) and normalization by
27
28 quantile sketch (Bolstad, et al., 2003). To assess differential expression at gene-level,
29
30 we used an empirical Bayes method (Smyth, 2004) together with a false discovery
31
32 rate (FDR) correction of the p-value (Westfall PH, 1993). Thus, the list of
33
34 differentially expressed genes was generated using an $FDR \leq 0.05$ together with an
35
36 absolute $\log_2(\text{fold-change})$ threshold of 1. Differential expression was detected by
37
38 linear model statistics. This method is based on the fitting of a linear model to
39
40 estimate the variability in the data. In case of one-channel microarray data this
41
42 approach is the same as the analysis of variance except that a model is fitted for every
43
44 gene. For the detection of the differential expression an empirical Bayes method is
45
46 used to moderate the standard errors. The use of moderated statistics for the detection
47
48 of differential expression is especially useful in cases of experiments with a small
49
50 number of replicates.
51
52
53
54
55
56
57
58
59
60

1
2 Alternative splicing events (ASEs) were detected as described in (Della Beffa, et al.,
3 2008). Briefly, an intensity filter was applied at gene-level to remove not expressed
4 and low expressed genes, i.e. genes were retained for exon-level analysis if in all
5 biological replication gene-level signal was greater than 5. Subsequently, only genes
6 characterized to have at least two RNA isoforms annotated in Ensembl database
7 (Ensembl 56 release, September 2009, (Flicek, et al., 2008)) were retained for further
8 analysis. The Splicing Index value was calculated by taking the \log_2 ratio of the
9 normalized exon intensity (NI) in Sample 1 and the NI in Sample 2. The normalized
10 exon intensity (NI) is the ratio of the probe set intensity to the gene intensity.

11
12 The data discussed in this publication have been deposited in the NCBI Gene
13 Expression Omnibus (Edgar, et al., 2002) and are accessible through GEO Series
14 accession number GSE21450 embedding dataset SOD1 (GSE21298) and dataset PQ
15 (GSE21305).
16
17
18
19

20 21 22 23 24 25 26 27 28 29 30 31 *Quantitative RT-PCR assays*

32 For the experiments performed on cultured cells, the relative mRNA levels of selected
33 transcripts were determined by qPCR on three biological replicates and a pool of the
34 same RNA samples employed for the microarray experiments. 2 μg of total RNA
35 were reverse-transcribed using MultiScribeTM Reverse Transcriptase (Applied
36 Biosystems), random hexamers (Applied Biosystems), RNAsin Plus reagent
37 (Promega) and dNTPs for 2 h at 37°C according to manufacture's instruction. qPCR
38 amplifications were performed in a final volume of 25 μl with SYBR[®] Green qPCR
39 master mix (Applied Biosystems), 1 μl cDNA diluted (1:50), and 0.2 μM of each
40 primer (for sequences see Supporting Material, Table S8 "Oligonucleotide primers").
41
42
43
44
45
46
47
48
49
50
51
52
53
54

1
2
3
4
5
6
7
8
9
10
11
12
13
14
15
16
17
18
19
20
21
22
23
24
25
26
27
28
29
30
31
32
33
34
35
36
37
38
39
40
41
42
43
44
45
46
47
48
49
50
51
52
53
54
55
56
57
58
59
60

Amplifications were performed in duplicate or triplicate using an ABI PRISM 7500 real time system (Applied Biosystems). The amplification protocol was as follows: an initial denaturation and activation step at 95°C for 10 min, followed by 40 cycles of 95°C for 15 s and 60°C for 1 min. After the amplification phase, a dissociation step was carried out at 95°C for 15 s, 60°C for 1 min, and 95°C for 15 s. For normalization of cDNA loading, all samples were run in parallel using GAPDH as housekeeping gene for human samples and Hprt1 for mouse samples. To estimate primer efficiencies, a standard curve was generated for each primer pair from 10-fold serial dilutions (from 20 to 0.002 ng) of a pool of first-stranded cDNA template from all samples. Standard curves represented the cycle threshold (Ct) value as a function of the logarithm of the number of copies generated. All real-time PCR efficiencies were above 85%. Values of relative expression in neuroblastoma cells [(treated with PQ vs. untreated or G93A-SOD1 vs. WT-SOD1] or mouse tissues (brain or spinal cord from transgenic vs. control) were statistically analyzed by two tailed t-test.

The data of the expression analysis on mouse spinal RNA during disease progression was analyzed using a linear regression model and plotted as $\Delta Ct(\text{transcript-Hprt1})$ vs. age. Statistical analysis was performed using SPSS software (SPSS Inc.). Wasf3 and Sept2 expression data were grouped into different stages (pre-onset: 93, 103, and 113 days; onset: 135 days; symptomatic stage: 140 - 170 days) and plotted as $1/2^{\Delta Ct(\text{transcript-Hprt1})}$ vs. phases (pre-onset phase: Ntg: n=6, G93A: n=5; early phase Ntg: n=2, G93A: n=2; symptomatic phase: Ntg: n=3, G93A: n=7).

Alternative splicing events validation by RT-PCR

Validation of splicing changes predicted by microarray experiments was performed by RT-PCR analysis on a pool of the RNA samples used for array hybridization and

1
2 on 3 other independent preparations. cDNA synthesis was performed as described
3
4 above. Assay conditions were optimized for each gene with respect to primer
5
6 annealing temperatures, primer concentration, and MgCl₂ concentrations. The
7
8 number of amplification cycles used for each reaction was determined to ensure that
9
10 transcript amplification was within a linear range (25 to 35 cycles). Gene specific
11
12 primer sequences are listed in Supporting Material, Table S8. PCR products were
13
14 separated by electrophoresis on 2-4% agarose gels. Quantification was performed
15
16 with a 2100 Bioanalyzer (Agilent Technologies). Statistical analysis was performed
17
18 using GraphPad InStat software (GraphPad Software Inc.). The amplified PCR
19
20 products were cloned in pGEM T Easy Vector System (Promega, Madison, USA) and
21
22 sequenced by BMR Genomics.
23
24
25

26 *Immunoblotting*

27
28 Cell monolayers were washed twice with ice cold PBS and lysed on the tissue culture
29
30 dish by addition of ice-cold lysis buffer (50mM Tris-HCl, pH 7.5, 150mM NaCl, and
31
32 1% NP-40, and complete protease inhibitor cocktail (Roche Diagnostics). The
33
34 samples were then centrifuged at 15,000 rcf for 15 min at 4°C, and the supernatants
35
36 were collected. An aliquot of the cell lysate was used for protein analysis with the
37
38 Bio-Rad Bradford kit for protein quantification. Proteins were subjected to SDS-
39
40 PAGE and then transferred onto nitrocellulose membrane (Thermo Fisher Scientific).
41
42 The membranes was blocked for 1 h with 5% non-fat dry milk in PBS-buffered saline
43
44 containing 1% Tween 20 (PBS-T). Membranes were immunoblotted with antibodies
45
46 of interest for 1 h. Anti-cyclin A , and anti-cyclin B, were from BD Biosciences,
47
48 (Pharmingen). The anti-NTRK1 (TrkA) antibody was from Abcam.
49
50
51
52
53
54
55
56
57
58
59
60

1
2
3 For the analysis of semaphorin 3A expression, 10^6 cells were plated on 60 mm Petri
4
5 dishes. After 24hrs culture in normal growth medium, cells were shifted in 3ml
6
7 OPTIMEM (Invitrogen) and cultured for 18hrs. Supernatants were harvested,
8
9 centrifuged to remove cell debris, and 200ml of cleared supernatants were precipitated
10
11 with 6 volumes of a 2:1:1 Ethanol/Methanol/Acetone mix and resuspended in
12
13 Laemmli sample buffer. Equal volumes were subjected to SDS-PAGE and analysed in
14
15 Western blot with an anti-SEMA3A mouse monoclonal antibody (Santa Cruz
16
17 Biotechnology Inc.). To normalize the amounts of secreted SEMA3A to the cell
18
19 number, cells were lysed in RIPA buffer and equivalent amounts of protein extracts
20
21 were analysed in Western blot with a mouse monoclonal anti-b-actin antibody
22
23 (Sigma-Aldrich).

24
25 The detection was carried out by incubation with horseradish peroxidase conjugated
26
27 sheep anti-mouse IgG (Amersham) for 1 h. The blots were then washed extensively
28
29 and the proteins visualized using an enhanced chemiluminescent detection system
30
31 (Amersham).

32 33 34 *Animals*

35
36 Transgenic mice expressing the human *SOD1* gene with the G93A mutation (strain
37
38 B6.Cg-Tg(*Sod1*-G93A)1Gur=J, Gurney, et al., 1994) were purchased from the
39
40 Jackson Laboratory (Bar Harbor, ME). Transgenic females were used for RNA
41
42 extraction and compared to age-matched non-transgenic females. The same operator
43
44 who was blind to the genotype of mice tested all animals twice a week for deficit in
45
46 grip strength, Rotarod performance and body weight. The progressive body weight
47
48 loss was calculated as the difference from the maximum weight recorded for each
49
50 animal. Analyses started at 30 days (progressive body weight) and 12 weeks (motor
51
52
53
54
55
56
57
58
59
60

1
2 performances) of age. Rotarod testing was performed using the accelerating Rotarod
3 apparatus (Ugo Basile 7650 model). The onset of clear symptoms was considered
4 when the mice showed the first impairment in grip strength. The symptomatic phase
5 stage of disease was considered when the mice showed a 10% weight loss that was
6 usually accompanied with the first impairment in Rotarod performance. All animal
7 studies were conducted in accordance with standard ethical guidelines
8
9
10
11
12
13
14
15

16 **Results**

17
18 The fact that neurons are highly dependent on the oxidative energy metabolism has
19 suggested a common pathogenic mechanism for neurodegeneration based on an
20 underlying dysfunction in mitochondrial activity. To investigate the cellular response
21 to mitochondrial insufficiency both at the level of gene expression and at the pre-
22 mRNA splicing level we performed a whole-genome, splicing-sensitive microarray
23 analysis of two experimental paradigms. First, we profiled untreated human
24 neuroblastoma SH-SY5Y cells vs. cells treated with PQ. PQ is a neurotoxic herbicide
25 that belongs to the class of redox cycling compounds capable of inducing
26 mitochondrial damage, increasing reactive oxygen species (ROS) production and
27 oxidative stress (Birney, et al., 2007; Castello, et al., 2007). For this experiment, the
28 most effective PQ concentration was determined by concentration–response time
29 course studies using an MTT assay to monitor mitochondrial activity, and RT-PCR to
30 verify alternative splicing changes of endogenous transcripts (see Supporting Results).
31
32 Second, we analyzed SH-SY5Y cells stably expressing wild type SOD1 (WT-SOD1)
33 vs. cells expressing a pathogenic mutation (G93A-SOD1, (Carri, et al., 1997). We
34 have previously demonstrated that this mutant SOD1 induces mitochondrial defects
35 such as depolarization, impaired respiratory activity and ATP production, altered
36
37
38
39
40
41
42
43
44
45
46
47
48
49
50
51
52
53
54
55
56
57
58
59
60

1
2 calcium buffering and cytochrome c release in this and other neuronal cell lines
3
4 (Cozzolino, et al., 2009; Ferri, et al., 2006; Jaiswal, et al., 2009). Mitochondrial
5
6 damage has been repeatedly reported also in transgenic mice overexpressing
7
8 Sod1G93A (Damiano, et al., 2006; Jaiswal and Keller, 2009; Mattiazzi, et al., 2002;
9
10 Nguyen, et al., 2009). In this experiment, WT-SOD1 cells were used as a control to
11
12 rule out unspecific effects due to the transfection and/or to an increased level of SOD1
13
14 activity.

15
16 After having assessed their quality (see Supporting Material), biologic quintuplicate
17
18 RNA samples prepared from each experimental paradigm were hybridized to Human
19
20 Exon 1.0 ST Arrays (Affymetrix), which allow the definition of both transcription
21
22 patterns (gene-level analysis) and alternative pre-mRNA maturation events (exon-
23
24 level analysis). Probesets on the Exon Array are classified as Core, Extended, or Full
25
26 according to the reliability of the annotation used to define the putative genomic
27
28 regions of interest. All analyses reported here utilized only the highest confidence
29
30 “core” probesets, which are based on RefSeq and GenBank full-length mRNAs.
31
32 Probesets are grouped into “transcript clusters” corresponding to all possible isoforms
33
34 transcribed from a single locus or gene; therefore, for simplicity we refer to transcript
35
36 clusters as genes throughout these results. As illustrated in Figure 1A, gene-level and
37
38 exon-level data sets were generated for each experiment. Hierarchical clustering
39
40 showed good segregation of treated samples from control samples (PQ vs. untreated
41
42 and G93A-SOD1 vs. WT-SOD1, respectively (Figure 1B). Sample group
43
44 homogeneity was also confirmed by Principal Component Analysis (not shown)
45
46 Differential expression was detected by linear model statistics (see Materials and
47
48 Methods, (Smyth, 2004)). Exon-level calculation was done by RMA (Irizarry, et al.,
49
50 2003) and normalization by quantile sketch (Bolstad, et al., 2003). Also in this case
51
52
53
54

1
2 hierarchical cluster analysis showed a good correlation between the two experimental
3
4 groups (Figure 1C).
5

6
7
8 *Gene-level expression profiling reveals extensive transcriptional changes upon*
9 *mitochondrial dysfunction*

10
11 We first analyzed gene expression changes in PQ-treated cells. To identify
12 differentially expressed genes we applied, as cut off an absolute \log_2 -fold change $\geq \pm 1$
13 and a p-value ≤ 0.05 . Among the 790 genes that were differentially expressed in the
14 treated samples compared with the controls, 403 were upregulated and 387 were
15 downregulated (Supporting Material, Supp. Table S1 “Paraquat gene-level analysis”).
16
17 The selected genes were analyzed for their molecular and cellular functions and
18 involved pathways using the Ingenuity Pathways Analysis software (IPA7.0,
19 Ingenuity Systems®). The analysis identified *Cellular Growth and Proliferation*, *Cell*
20 *Death*, and *Cell Cycle*, as the top three categories among the known affected
21 biological functions (Table 1). Consistent with the idea that oxidative stress is a
22 critical mechanism in PQ-induced neurotoxicity (Castello, et al., 2007), IPA 7.0
23 analysis identified 29 genes that are associated with oxidative stress (Table 2).
24
25 However, the dominant pathway affected by PQ treatment was p53 signalling. The
26 activation of the p53-mediated response is indicated by the upregulation of *ATF3*,
27 *BTG2*, *CDKN1A*, *GADD45A/B/G*, *MDM2*, *PPM1D*, *SESN1/2*, *TP53INP1*, and by
28 *POLH* (for gene name abbreviations see Supp. Table S8).
29
30
31
32
33
34
35
36
37
38
39
40
41
42
43
44

45 Next, we carried out whole-genome profiling of SH-SY5Y cells stably transfected
46 with cDNAs coding for WT-SOD1 or the mutant G93A-SOD1 protein. Among the
47 192 genes that were found to be differentially expressed in the G93A-SOD1 samples,
48 81 were upregulated and 111 were down-regulated (Supp. Table S2 “SOD gene-level
49
50
51
52
53
54

1
2
3 analysis”). Analysis of the selected genes with IPA7.0 identified *Cellular Movement*
4 as top affected molecular and cellular function, *Nervous System Development* as top
5 affected function related to “Physiological System Development and Function”, and
6
7
8
9
10
11
12
13 *Genetic Disorders, Neurological Diseases* and *Psychological Diseases* as the top
14 three categories among the affected functions related to “Diseases and Disorders”
15 (Table 3).

16
17 In order to identify common deregulated pathways, we then combined those genes
18 from the two data sets, which were characterized by an absolute \log_2 -fold change \geq
19 0.5 and by an uncorrected p-value ≤ 0.05 . This intersection resulted in the detection of
20 156 genes that were differentially expressed in both conditions (Supp. Table S5
21
22 “Common gene-level analysis”, and Figure 1D). These genes were used to query the
23
24 Ingenuity IPA 7.0 knowledge database. The analysis identified *Nervous System*
25
26
27
28
29
30
31
32
33
34
35
36
37
38
39
40
41
42
43
44
45
46
47
48
49
50
51
52
53
54
55
56
57
58
59
60
Development and Function as the top affected biological function (Table 4).
Moreover, 28 genes were found to be associated to neurological disorders, 8 to axonal
guidance signalling, 2 to glycosphingolipid biosynthesis, and 3 to the glycerolipid
metabolism (Supp. Table S6). Additional genes involved in neuritogenesis were
differentially expressed in only one of the two data sets (Supp. Table S6).

Exon-level profiling reveals the expression of alternative mRNA isoforms

Array data were next examined for evidence of differential exon expression, i. e.
alternative pre-mRNA splicing. To remove low intensity signals only genes
characterized by $\log_2 \geq 5$ were considered. Moreover, analysis was restricted to 4148
transcripts characterized by having at least two mRNA isoforms annotated in the
Ensembl database. Exon probesets intensity signals were normalized with respect to
gene-level signals to generate “splicing index” values (see Materials and Methods).

1
2 Differentially expressed exon probe sets, i.e. putative alternative splicing events
3 (ASEs), were detected according to Della Beffa et al. (Della Beffa, et al., 2008). The
4 integration of the results of MiDAS (Gardina, et al., 2006) and Rank Product
5 (Breitling, et al., 2004) characterized by a $p \leq 0.05$ lead to the identification of 816
6 putative ASEs, associated to 521 genes (Supp. Table S3 “PQ-ASEs”). Analysis with
7 IPA 7.0 identified *Cellular Growth and Proliferation*, *Cell Death*, and *Cell Cycle* as
8 the most affected cellular and molecular functions (Table 5).
9

10 A similar analysis was performed for the G93A-SOD1 experiment. A total of 406
11 putative ASEs, associated to 242 genes were eventually identified (Supporting
12 Material, Table S4 “SOD1 ASEs”). In this case, pathway analysis detected *Calcium*
13 *Signaling*, *cAMP-mediated Signaling*, and *G-Protein Coupled Receptor Signaling* as
14 the most affected top canonical pathways (Table 6). Therefore from the *in silico*
15 analysis of the alternative splicing data, the two experimental paradigms appear to
16 differentially affect pre-mRNA splicing. Indeed, the integration of the two exon-level
17 datasets led to the identification of only 48 common ASEs associated to 40 genes
18 (Supp. Table S7, “Common ASEs”). Interestingly, 10 of these common genes
19 function in *Cellular Movement*. Finally, we examined the position of the alternatively
20 spliced exons with respect to their position in RefSeq transcripts. We classified exons
21 as initial, internal or last. According to this classification 14 events affected initial
22 exons, 3 occurred in terminal exons, and 24 fell in internal exons. Seven events could
23 either not be assigned or occurred in intronic positions. Interestingly, 9 events
24 (18,7%) reflected the possible use of alternative promoters. This observation is
25 consistent with the result of the analyses of the ENCODE regions (Birney, et al.,
26 2007), which identified >20% of genes having functional alternative promoters
27 (Cooper, et al., 2006). Finally, 18 out of 40 common AS genes are also differentially
28
29
30
31
32
33
34
35
36
37
38
39
40
41
42
43
44
45
46
47
48
49
50
51
52
53
54

1
2
3
4
5
6
7
8
9
10
11
12
13
14
15
16
17
18
19
20
21
22
23
24
25
26
27
28
29
30
31
32
33
34
35
36
37
38
39
40
41
42
43
44
45
46
47
48
49
50
51
52
53
54
55
56
57
58
59
60

expressed. However, of these only 50% undergo putative ASEs affecting internal exons. This result is consistent with previous reports that suggest that regulation of AS of cassette exons and regulation of transcription appear to act on separate genes (Pan, et al., 2004).

Experimental validation of the gene-level analysis of the microarray data confirmed altered expression of axon guidance genes

We first performed the experimental validation of the gene expression data obtained from the PQ experiment. Different cellular and biochemical approaches confirmed the soundness of the microarray data and the biological significance of the pathways identified with IPA 7.0 (see Supporting Material “Results” and Supp. Figure S1). For the validation of the gene-level data obtained from the intersection of the two experimental paradigms we chose twelve of the 156 differentially expressed genes that showed a common trend upon PQ treatment and in G93A-SOD1 cells. Genes were prioritized by fold change variation and functional classification. Specifically, we focused on genes encoding molecules involved in the *Nervous System Development and Function* category. Expression of these genes was analyzed by quantitative real-time reverse-transcriptase polymerase chain reaction (RT-qPCR). As shown in Figure 2, qRT-PCR data were in good agreement to the microarray results for all genes except for *VSNL1* and *ADAMTS1*.

As mentioned above, pathway analysis of the genes that showed a common trend in the two experimental paradigms identified eight genes involved in axon guidance signalling (Supp. Table S6). Additional axon guidance genes were differentially expressed in only one of the two dataset. More genes related to different aspects of neuritogenesis (transcription regulation of axon guidance molecules, intracellular

1
2 signalling, etc.) were also found differentially expressed in both data sets. To identify
3
4 molecular interactions among these genes we analyzed them further by IPA 7.0. The
5
6 Ingenuity program can convert data sets into networks containing direct and indirect
7
8 relationships between genes based on known interactions in the literature. The
9
10 software is capable not only of constructing associations of genes identified by
11
12 microarray (including relative expression levels), but also of predicting involvement
13
14 of additional molecules not associated with significant transcriptional changes. We
15
16 thus compiled a list of genes related to neuritogenesis from which the Ingenuity
17
18 software created a network, on which our transcriptomics data were overlaid. In this
19
20 network the 24 genes that were differentially expressed in our data sets were
21
22 connected to 16 additional genes (Figure 3A). The network contained several
23
24 transcription factors that are interconnected and involved in neuronal commitment and
25
26 differentiation (*ASCL1*, *ERBB3/4*, *NEUROG3*, *NKX2.2*, and *PAX6*). Of these genes,
27
28 *NKX2.2*, and *PAX6* have been shown to play crucial roles in controlling the timing of
29
30 neuritogenesis and gliogenesis in the developing ventral spinal cord modulating the
31
32 activities of the proneural factors *NEUROG1/2/3*, and *ASCL1* (Sugimori, et al., 2007).
33
34 Interestingly, *ASCL1* is strongly downregulated both in PQ-treated and in G93A–
35
36 SOD1 cells. In addition, the network connected genes encoding cytoplasmic proteins
37
38 that may regulate actin dynamics such as *WASF3* and *EVL*.

39
40 Hierarchical cluster analyses of the expression data of the subset of genes involved in
41
42 neuritogenesis identified the majority of them as being downregulated (Figure 3B).
43
44 qPCR analysis of a subset of these genes confirmed the array data (Figure 3C). We
45
46 also tested by Western blotting the level of SEMA3A in the supernatant of PQ-treated
47
48 and G93A-SOD1 cells as well as the expression of NTRK1. As shown in Figure 3D
49
50 and 3E, these experiments confirmed the increased expression of the repulsive
51
52
53
54

1
2
3
4
5
6
7
8
9
10
11
12
13
14
15
16
17
18
19
20
21
22
23
24
25
26
27
28
29
30
31
32
33
34
35
36
37
38
39
40
41
42
43
44
45
46
47
48
49
50
51
52
53
54
55
56
57
58
59
60

SEMA3A and the downregulation of the neurotrophin receptor NTRK1 in both our models of mitochondrial dysfunction. Taken together these results suggest the formation of an altered, possibly more chemorepulsive cell environment.

Altered expression of genes involved in neuritogenesis in G93A-Sod1 mice

To determine whether changes in the expression of genes involved in axon growth and guidance could be observed in an animal model of neurodegeneration, we investigated the expression of a subset of the identified genes in the G93A-Sod1 mouse model of ALS. Disease onset in our strain is around 120 days (Pizzasegola, et al., 2009). Thirteen of the differentially expressed genes involved in neuritogenesis were analyzed by RT-qPCR on RNA extracted from spinal cord and brain of four transgenic mice carrying the G93A-Sod1 mutation and three normal control littermates at 150 d. As shown in Figure 4A, this study confirmed the differential expression of Hgf, Cxcr4, and Sema3A in the spinal cord of symptomatic G93A-Sod1 mice. Thus, we decided to further characterize the alteration in the expression of eleven genes in the spinal cord of G93A-Sod1 mice during disease progression. We analyzed by RT-qPCR the expression profile of some of the genes identified in the microarray analysis (*Cxcr4*, *Hgf*, *Ntrk1*, *Prph1*, *Sema3A*, and *Wasf3*) and also of additional genes inferred from the literature (*Nrp2*, and *Sept2*) at the pre-onset (93, 103, and 113 days), onset (135 days), and symptomatic stage (140 - 170 days). Expression of Cxcr4 and Hgf increased significantly over time during disease course ($p=0.01$ for Cxcr4., and $p<0.001$ for Hgf, Figure 4B), while Wasf3 and Sept2 showed increased expression in spinal cord of G93A-Sod1 mice at early symptomatic stage (Figure 4C).

Experimental validation of alternative splicing events

Next, we went on to confirm the putative ASEs identified by the exon-level analysis.

We chose ASEs affecting 15 transcripts involved in the top canonical pathways identified with IPA 7.0. In particular, we focused on genes involved in *Nervous System Development and Function*, which appeared to be affected by AS changes in either one, or both experimental paradigms. The location of the differentially expressed exon-probe set was manually inspected with the X:map software (Okoniewski, et al., 2007; Yates, et al., 2008) to determine its position on the transcripts annotated in Ensembl. Only ASEs occurring in exons for which there is at least one annotated alternative isoform were subjected to experimental validation by RT-PCR. All the amplified fragments were subcloned and sequenced to verify the identity of the splicing isoforms.

The Human Exon 1.0 ST array can identify mRNA variants that differ in the use of exons, introns, promoters and polyadenylation sites. In the case of the *RPRDIA* gene the microarray data predicted an increased inclusion of exon 8 (identified by the probe set n. 3874170, boxed in Figure 5A). In the Ensembl database there are four transcripts annotated for this gene, one of which contains exon 8. To validate this ASE, RT-PCR analysis was performed with two forward primers (in exons 8 and 9) and a single reverse primer in exon 5 (Figure 5B). As shown in Figure 5C, RT-PCR confirmed the expected inclusion of exon 8 in G93A-*SOD1* cells.

Two potential ASE were also predicted to occur in the *BINI* gene. Specifically, microarray data predicted inclusion of exon 7 and skipping of exon 15 in PQ-treated cells. In G93A-*SOD1* cells the array data predicted inclusion of exon 15. To validate these ASEs, we amplified by PCR the relevant region of each mRNA using primers in

1
2
3
4
5
6
7
8
9
10
11
12
13
14
15
16
17
18
19
20
21
22
23
24
25
26
27
28
29
30
31
32
33
34
35
36
37
38
39
40
41
42
43
44
45
46
47
48
49
50
51
52
53
54
55
56
57
58
59
60

constitutive flanking exons (Figure 5, panels D to F). Sequencing of the PCR fragments confirmed the inclusion of exon 7. Unfortunately, we could not detect the event affecting exon 15. Instead, we observed a splicing switch affecting exons 14 and 16, which was not predicted by the array. The presence of some discrepancies between microarray data and RT-PCR is due to the limited statistical power of an exon-level analysis. We tried to address this issue by using 5 biological replicates for each microarray experiment and by reducing the number of tested hypotheses, focusing the analysis only on expressed exons associated to annotated mRNA isoforms. Nevertheless, the multiple testing problem remains a critical issue in the exon-level analysis of array data (Della Beffa, et al., 2008). Additional ASEs in internal exons were confirmed for *GNAO1* (Figure 4G) and for *NRG1* (data not shown).

Among the probe sets exhibiting changes in expression, several mapped to the 5' end of the transcripts and were considered to be candidate alternative first exons. We considered the case of the *ABLIM1* gene for which several different alternatively spliced transcripts have been identified, some of them most likely transcribed from alternative promoters (Figure 6A). The probe set intensities along the entire *ABLIM1* gene are shown in Figure 6B. The exon array data predicted the skipping of an internal first exon in both experimental paradigms exon (boxed in Fig. 6B, see also the schematic representations in panels 6A and 6C). To validate this event we performed a semiquantitative PCR with two forward primers and a single reverse primer. This type of competitive PCR reactions have been used previously to detect variations in expression of 5'- and 3'-terminal exons (Karni, et al., 2007; Yamamoto, et al., 2009). As shown in Figure 6C, both upon PQ treatment and in G93A-*SOD1* cells the amount of the PCR fragment corresponding to the mRNA transcribed from

1
2 the distal promoter increased relative to the shorter fragment corresponding to the
3 mRNA transcribed from the alternative, internal promoter, thus confirming the
4 microarray prediction.
5
6
7

8 Three additional examples of alternative first exon usage that were similarly predicted
9 by the exon array data were verified by RT-PCR (*CHN1*, *LMO3*, and *NRG1*, Figure
10 6D). In the case of the *CHN1* gene, the skipping of an alternative first exon upon PQ
11 treatment and its inclusion in *G93A-SOD1* cells was confirmed by qPCR (Figure 6E)
12
13 The switches in first exon usage for *ABLIM1*, *CHN1*, and *NRG1* strongly influence
14 the coding potential of the different mRNA isoforms (Figure 6F). In the case of the
15 *ABLIM1* gene, we observed an increase of the longer transcript variant, which
16 encodes a protein that contains four LIM domains. These domains are not present in
17 the isoform encoded by the mRNA variant transcribed from the internal first exon.
18
19 Similarly, the short *CHN1* isoform that is differentially expressed upon PQ treatment
20 and in *SOD1(G93A)* cells lacks an SH2 domain. In contrast, the switch of first exons
21 in the *LMO3* gene results in different 5' UTR sequences for the different transcripts.
22
23
24
25
26
27
28
29
30
31
32
33

34 Discussion

35 In this study we sought to contribute to the understanding of the link between
36 mitochondrial stress and neurodegeneration. To this end we performed a whole-
37 genome analysis using splicing-sensitive microarrays of two different cellular
38 paradigms of mitochondrial dysfunction. First, we profiled human SH-SY5Y
39 neuroblastoma cells untreated or treated with PQ, a redox cycling molecule that
40 induces mitochondrial damage. Second, we compared SH-SY5Y cells stably
41 expressing wild type *SOD1* to cells expressing the mutant *G93A-SOD1* protein.
42
43 Mutations in *SOD1* are one of the genetic causes of ALS. The mutant proteins have
44
45
46
47
48
49
50
51
52
53
54

1
2
3
4
5
6
7
8
9
10
11
12
13
14
15
16
17
18
19
20
21
22
23
24
25
26
27
28
29
30
31
32
33
34
35
36
37
38
39
40
41
42
43
44
45
46
47
48
49
50
51
52
53
54
55
56
57
58
59
60

been found in mitochondria and are believed to cause multiple damages (for review see (Shi, et al.). The data sets from the two experimental paradigms were then integrated in order to identify common deregulated genes.

Our findings indicate that mitochondrial damage can induce profound changes in the expression of genes involved in relevant pathways for neuronal survival, both at the gene-level and in pre-mRNA splicing. In addition to previously described changes in the expression of cytoskeletal and molecular motor proteins (“*Cell Movement*”), we identified alterations of a subset of genes involved in *Nervous System Development and Function*, including axon growth and guidance genes, and genes encoding proteins involved in synaptic vesicles formation. Changes in the expression of a subset of the identified genes were confirmed in the G93A-*Sod1* mouse, a model for ALS, supporting the idea that alterations in the expression of this category of genes may contribute to explain the vulnerability of synapses and distal axons observed in many neurodegenerative diseases (for review see (Conforti, et al., 2007).

Cell Movement

Recent studies have shown that neurons in general, and even more so motor neurons, are highly sensitive to defects in axonal transport due to their extreme polarization. Decreased kinesin-mediated (anterograde) and dynein-mediated (retrograde) axonal transport have been observed both in ALS patients and in transgenic animal models (for review see (De Vos, et al., 2008; Strom, et al., 2008)). In G93A-*Sod1* transgenic mice, a considerable inhibition of retrograde axonal transport was observed at a very early stage of disease before animals became symptomatic (Jiang, et al., 2005). We observed downregulation of several members of the kinesin family in both experimental paradigms. In the G93A-*SOD1* experiment is particularly noteworthy

1
2 the downregulation of KIF1A, an anterograde motor protein. Altered expression of
3 KIF1A had already been reported in 75-days old G86R-Sod1 mice (Dupuis, et al.,
4 2000). The phenotype of *Kif1A* knockout mice includes motor and sensory
5 disturbances, a reduction in the density of synaptic vesicles in nerve terminals, and
6 accumulation of clear vesicles in nerve cell bodies (Yonekawa, et al., 1998). KIF1A
7 cargos include a subset of precursors for synaptic vesicles: synaptophysin,
8 synaptotagmin, and Rab3A. In this context it should be mentioned that we also
9 observed altered expression of several genes involved in synaptic function including
10 three members of the synaptotagmin family (*SYT2*, *SYT4*, and *SYT12*, which encode
11 integral membrane proteins of synaptic vesicles), synaptojanin-2 (*SYNJ2*, coding for a
12 phosphoinositide phosphatase implicated in cytoskeletal dynamics during
13 endocytosis) as well as genes encoding components of the presynaptic active zone
14 (*RIM1*, and *RIM3*). Consistent with these data, pre-degenerative depletion of synaptic
15 vesicles has been reported in ALS (Pun, et al., 2006).

16
17
18
19
20
21
22
23
24
25
26
27
28
29
30 In G93A-*SOD1* cells, we also observed downregulation myosin X (*MYO10*) coding
31 for another molecular motor, while PQ treatment induced upregulation of *MYLIP*
32 (myosin regulatory light chain interacting protein). *MYLIP* is expressed in the cell
33 bodies and growth cones of rat embryonic hippocampal neurons, and belongs to a
34 family of cytoskeletal effector proteins that link actin to membrane-bound proteins at
35 the cell surface. Interestingly, in rat PC12 neural precursor cells, *MYLIP*
36 overexpression inhibited NGF-induced neurite outgrowth (Olsson, et al., 2000;
37 Olsson, et al., 1999). Overall, these data reinforce the concept that alteration of axonal
38 transport is involved in neurodegeneration, and suggest that this alteration may
39 descend directly from mitochondrial damage.
40
41
42
43
44
45
46
47
48
49
50

Nervous System Development and Function

As mentioned above, pathway analysis of the genes that were differentially expressed in both experimental paradigms highlighted several genes associated to axon guidance (Supp. Table S6). Axon guidance is a partially understood process that has a major role not only in embryonic development (O'Donnell, et al., 2009) but in the maintenance of the mature peripheral nervous system as well (Yoo, et al., 2009). Several lines of evidence support the hypothesis that aberrant expression of axon guidance proteins such as Semaphorins, Ephrins, Netrins and Slits, may induce pathological changes in motor neurons and contribute to the pathogenesis of ALS ((Schmidt, et al., 2009). Both in PQ-treated cells as well as in G93A-SOD1 cells we observed downregulation of SEMA6A and of its receptor PLXNA4. Moreover, SEMA3D is among the top upregulated genes in both datasets. This semaphorin is expressed at the dorsal spinal cord midline and appears to guide axons by repulsion and modulation of fasciculation (Wolman, et al., 2004).

Additional genes coding for axon guidance molecules were differentially expressed in either one of the two experimental paradigms. For example, in G93A-SOD1 cells we observed upregulation of neuropilin 2 (*NRP2*), coding for a selective receptor for class 3 semaphorins that is required for the development of central nervous system and peripheral nervous system projections (Giger, et al., 2000), and of SEMA3A, a chemorepellant for cortical axons and an inhibitor of axonal regeneration and other regenerative responses after spinal cord injury (Kaneko, et al., 2006).

Paraquat treatment induced downregulation of *SEMA3F*, and *SEMA6D*. Interestingly, an association between *SEMA6A* polymorphisms and ALS has previously been reported (Lesnick, et al., 2008). Also noteworthy is the reduction in NTRK1 expression, a neurotrophin receptor that is thought to play a role in axon guidance and

1
2
3
4
5
6
7
8
9
10
11
12
13
14
15
16
17
18
19
20
21
22
23
24
25
26
27
28
29
30
31
32
33
34
35
36
37
38
39
40
41
42
43
44
45
46
47
48
49
50
51
52
53
54
55
56
57
58
59
60

outgrowth in conjunction with SEMA3A. In addition, we observed reduced expression of *SDC2*, coding for a member of the heparan sulphate proteoglycan (HSPG) family of extracellular matrix proteins both in PQ-treated and in G93A-*SOD1* cells. Some axon guidance molecules bind to HSPGs, and this modulates their repulsive properties (Jokic, et al., 2006). Thus, the downregulation of *SDC2* might suggest a shift to a more repulsive character of the extracellular matrix. This effect is possibly aggravated by the upregulation of *SEMA3D* and the downregulation of *SEMA6A*.

In both experimental paradigms we observed altered expression not only of classical members of the ligand/receptor axon guidance systems but also of genes involved in a broader sense in neuritogenesis, such as genes encoding downstream intracellular signal transduction molecules and upstream transcription factors that control axonal patterning (for review see O'Donnell, et al., 2009; Polleux, et al., 2007). For example, in G93A-*SOD1* cells we observed upregulation of *RGNEF* (Rho-guanine nucleotide exchange factor). *RGNEF* is a human homologue of mouse p190RhoGEF, a low molecular weight neurofilament (NFL) mRNA stability factor that was shown to be involved in NF aggregate formation in neurons (Lin, et al., 2005; Volkening, et al., 2009). In PQ-treated cells we found the downregulation of three genes (*ISL1*, *LHX8*, and *LHX9*) that belong to the family of LIM homeobox transcription factors. It has been shown that in the developing mouse spinal cord *Isl1* and *Lhx1* control the dorsoventral specificity of motor axon projections at least in part by controlling the expression of *EphA4* (Kania, et al., 2000). Interestingly, *LHX9* is also downregulated in G93A-*SOD1* cells.

A validation of the microarray data in G93A-*Sod1* mice confirmed the alterations in the expression of neuritogenesis genes during disease progression. For example, we

1
2 observed a progressive increase in the expression of *Hgf* during disease course. HGF,
3 which has neurotrophic effects in the motor neurons and central nervous system, was
4 found to be upregulated in motor neurons of sporadic ALS patients (Jiang, et al.,
5 2005). In addition we found increased expression of *Cxcr4* from pre-symptomatic to
6 end-stage. CXCR4 and its ligand SDF1 regulate neural development by modulating
7 cell migration and axon growth and guidance and by promoting cell survival and
8 proliferation (Chalasani, et al., 2003; Stumm and Holtt, 2007; Zou, et al., 1998) .
9

10 Taken together, our data indicate that mitochondrial stress can induce transcriptional
11 alterations of multiple genes involved in neuritogenesis, and are in agreement with the
12 observation that dorsal root ganglia neurons from adult mice expressing G93A-Sod1
13 in culture grow shorter neurites (Perlson, et al., 2009). The idea that differential
14 expression of genes relating to the growth of neuronal processes, and formation of
15 synapses may play a role in neurodegeneration is supported by a recent microarray
16 analysis of spinal motor neurons of *Vegf^{fl/c}* mice, a different ALS mouse model
17 (Brockington, et al.). Since it has been observed that in neuromuscular diseases such
18 as ALS selective synaptic weakening and denervation start long before the actual
19 motor neuron loss, and prior to the appearance of clinical symptoms (Fischer, et al.,
20 2004), the expression of repulsive signals could act during the presymptomatic stages
21 and contribute to the retraction of axon terminals from the neuromuscular synapse
22 before the death of motor neurons occurs.
23
24
25
26
27
28
29
30
31
32
33
34
35
36
37
38
39
40
41
42

43 *Changes in alternative pre-mRNA splicing*

44 RNA-based mechanisms have been implicated in several neurodegenerative
45 conditions leading to the recognition of new pathogenic pathways (for review see
46 (Licatalosi and Darnell, 2006; Strong, 2009). In ALS, numerous reports have
47
48
49
50
51
52
53
54

1
2 highlighted differential expression of protein isoforms, which arise from AS events in
3 the affected tissues of patients, as well as in the mouse models (Aerbajinai, et al.,
4 2002; Munch, et al., 2002; Pantelidou, et al., 2007; Robertson, et al., 2003;
5 Tomiyama, et al., 2002). RNA processing has been further implicated in ALS
6 pathogenesis by the recent characterization of mutations in two DNA/RNA-binding
7 proteins (TDP43 and FUS/TLS) in familial and sporadic patients (for review see
8 (Lagier-Tourenne and Cleveland, 2009; Strong, 2009).

9
10 Exon-level analysis of our microarray data detected a widespread alteration in pre-
11 mRNA splicing. We selected for experimental validation events affecting genes
12 involved in the pathways mentioned above (i.e. *Cell Movement* and *Nervous System*
13 *Development and Function*). For example, the *ABLIM1* gene encodes a cytoskeletal
14 protein that binds to actin filaments. The *C. elegans* homolog UNC-115 was shown to
15 act as a downstream cytoskeletal effector of Rac signaling in axon pathfinding (Gitai,
16 et al., 2003; Struckhoff and Lundquist, 2003). Our data indicate that alternative
17 promoter usage modulates the ration between mRNAs encoding the full-length
18 protein or a shorter isoform lacking the LIM zinc-finger domain, which is thought to
19 mediate protein:protein interactions. A second example is provided by *CHN1*. This
20 gene codes for two different isoforms of a signaling protein implicated in the
21 pathfinding of corticospinal axons in mice brain (Brown, et al., 2004). Upon PQ
22 treatment we observed a decrease of the mRNA encoding the short isoform, and
23 therefore a relative increase in the expression of the long isoform. The two protein
24 isoforms share a RacGAP domain that interacts with and down-regulates Rac activity.
25 However, the long isoform (alpha2-chimerin) contains an N-terminal SH2 domain
26 that is not present in the short isoform, transcribed from an internal promoter. Shi et
27 al. showed that the longer isoform is required for EphA4 -dependent growth cone
28
29
30
31
32
33
34
35
36
37
38
39
40
41
42
43
44
45
46
47
48
49
50
51
52
53
54
55
56
57
58
59
60

collapse (Shi, et al., 2007). Finally, we observed changes in the alternative splicing pattern of BIN1. This was especially intriguing given the known interactions of BIN1 with dynamin in pre-synaptic membranes of the nervous system and its role in endocytic recycling (Leprince, et al., 2003; Nicot, et al., 2007; Pant, et al., 2009; Takei, et al., 1999). These findings suggest that mitochondrial dysfunction may have a severe effect not only on transcription but also on pre-mRNA splicing of a subset of genes that participate in biological processes that are relevant for neurodegeneration.

But how do these splicing changes arise? Expression of neuron-specific proteins involved in RNA splicing and metabolism is affected in several neurological disorders (Licatalosi and Darnell, 2006). Surprisingly, in our experiments we did not detect any differentially expressed gene encoding a splicing regulatory factor. The only gene coding for an RNA-binding protein, which is differentially expressed in both paradigms, is ELAVL2 (Supp. Table S5), one of the mammalian homologs of ELAV, a protein essential for neurogenesis in Drosophila (Robinow et al., 1988). ELAVL2 encodes the neuronal HuB protein that binds and stabilizes target mRNAs containing AU-rich elements (ARE) in the 3' UTR (for review see M. N. Hinmana and H. Lou, 2008). Instead, among the common ASEs (Supp. Table S7) we found CUGBP2, a well-known alternative splicing factor (for review see Barreau, et al., 2006). CUG-BP2 is particularly relevant in the context of neurodegeneration since it has a specific neuromuscular expression and is differentially expressed in several models of SMA (Anderson, et al., 2004). The putative ASE affecting the CUGBP2 transcript occurs in the 3' UTR and may thus influence either intracellular localization or stability of the mRNA. This in turn may affect splicing, stability and/or translation of specific transcripts.

Deleted: N

Deleted: are

Deleted: However, i

Deleted: pre-mRNA

Deleted: s

Formatted

Deleted:

Formatted

Formatted

Formatted

Formatted

1
2
3 If mitochondria stress does not lead to extensive changes in the expression of splicing
4 regulatory proteins, AS alterations may be the consequence of post-translational
5 modifications of splicing regulatory proteins that change their activity and/or
6 intracellular distribution. Indeed, it has already been documented that different types
7 of cell stress (osmotic stress, heat-shock, or arsenite treatment) result in altered
8 phosphorylation and intracellular localization of members of the hnRNP and SR
9 families of splicing factors (for review see Biamonti and Caceres, 2009). It is clear
10 that alterations in the expression and activity induced by cellular stress are mediated
11 through the interplay of multiple signalling pathways. Which mechanisms of signal
12 transduction respond to mitochondrial stress thereby causing derangement of splicing
13 needs further elucidation.

14
15
16
17
18
19
20
21
22
23
24 In conclusion, whole genome exon level profiling of our cellular models has
25 identified neuritogenesis and axon guidance as relevant pathways specifically altered
26 by mitochondrial dysfunction. Dysregulation occurs at the level of both gene
27 expression and alternative pre-mRNA splicing. Genes controlling axon outgrowth and
28 guidance, and synapse formation play a fundamental role during embryonic
29 development in the establishment of functional circuits. However, they also function
30 in the mature mammalian CNS where many neurons retain a limited degree of
31 structural plasticity. Changes in neural connectivity and loss of synaptic contacts are a
32 unifying hallmark of neurodegenerative disorders. Further studies are needed to
33 determine whether a reduction of neurotrophic factors and the establishment of a
34 repulsive environment may contribute to axonal degeneration and cell death in these
35 disorders.
36
37
38
39
40
41
42
43
44
45
46
47
48
49
50
51
52
53
54

Deleted: Therefore, we can hypothesize that the

Deleted: in pre-mRNA splicing observed in our experimental paradigms of mitochondrial stress

Deleted: arise

Deleted: by

Deleted: thereby

Deleted: changing

Acknowledgements

This work was supported by grants from Fondazione Cariplo to T.A., S.B., and M.T.C., from MIUR-PRIN to S.B. and M.T.C., from EC 7FPs TOLERAGE 202156 and FIGHT 242210 to F. Zolezzi and D.B., and from Regione Piemonte to R.C.; F. Cordero is supported by a grant from Regione Piemonte/Università di Torino. We thank R. Ambrosini for help with the statistical analysis of the in vivo data, and D. Talarico for carefully reading the manuscript and for helpful suggestions.

Supporting Material

File 1. Assessment of RNA quality

File 2. Supporting Results and Methods

File 3. Assessment of RNA and arrays quality .

Table S1. “Paraquat gene-level analysis”

Table S2. “SOD1 gene-level analysis”

Table S3. “PQ exon-level analysis”

Table S4. “SOD1 exon-level analysis”

Table S5. “Common gene-level”

Table S6. Genes associated to *Neurological Disorder, Axonal Guidance Signaling, and Neuritogenesis*.

Table S7. “Common ASEs”

Table S8. Main Entrez Gene abbreviations used in the text

Table S9. Oligonucleotide primers

Figure Legends**Figure 1. Whole genome, splicing-sensitive microarray analysis of the cellular response to mitochondrial dysfunction.**

- A. Diagram of the experimental design.
- B. Gene-level hierarchical cluster analysis of untreated vs. PQ-samples and WT-SOD1 vs. G93A-SOD1 samples. The two dendrograms (sample level hierarchical clustering with average linkage) represent the relative distance between samples.
- C. Exon-level hierarchical cluster analysis of untreated vs. PQ-samples and WT-SOD1 vs. G93A-SOD1 samples.
- D. Venn diagram illustrating the overlap between differentially expressed genes in the PQ-experiment and in the G93A-SOD1 experiment.

Figure 2. Experimental validation of the gene-level microarray data in SH-SY5Y cells.

qPCR validation of array data from the PQ and G93A-SOD1 experiments. Assays were performed in triplicate from a pool of the RNA samples used for the microarray analysis and from two different RNA preparations.

Figure 3. Mitochondrial dysfunction alters expression and splicing of genes involved in axon growth and guidance.

- A. A gene-interaction network of genes related to axon growth and guidance. Transcriptomics data were overlaid on a genetic network generated with the Ingenuity Pathway Analysis 7.0 software. This diagram is a graphical representation of 24 genes (in green), whose expression is altered in our

1
2
3
4
5
6
7
8
9
10
11
12
13
14
15
16
17
18
19
20
21
22
23
24
25
26
27
28
29
30
31
32
33
34
35
36
37
38
39
40
41
42
43
44
45
46
47
48
49
50
51
52
53
54
55
56
57
58
59
60

experimental paradigms of mitochondrial dysfunction, and of 16 additional genes (in grey) that may be involved in various aspects of neuritogenesis. Gene products are represented as nodes, and the biological relationship between two nodes is represented as an edge (line). All edges are supported by at least one reference from the literature, a textbook, or canonical Material stored in the Ingenuity Pathways Knowledge Base. Solid lines between genes represent known direct molecular interactions, and dashed lines, known indirect molecular interactions. Nodes are displayed by using various shapes that represent the functional class of the gene product.

- B. Hierarchical cluster analysis of genes involved in axon growth and guidance whose expression is altered in the two experimental paradigms. The dendrograms represent the relative distance between samples (top) and between genes (left). Expression signal intensities are shown in red and green, indicating high and low expression, respectively. The Entrez GeneID is indicated on the right of each panel.
- C. qPCR validation of the expression of the microarray data for genes involved in axon growth and guidance in SH-SY5Y cells. Experiments were performed in triplicates on three biological replicates. The Y-axis is expressed as means±standard error (SE). Samples identified by two asterisks are considered very significant (p value = 0.001 to 0.01) while those labelled with one asterisk are considered significant (p value = 0.01 to 0.05).
- D. Western blot analysis of NTRK1 expression in untreated and PQ-treated SH-SY5Y cells (left panel) and in SH-SY5Y cells expressing wild type SOD1 or G93A-SOD1 (right panel). Expression of beta-actin was used as an internal control. Data are representative of three independent experiments.

1
2
3 E. Determination of SEMA3A expression in culture supernatants of untreated
4 and PQ-treated SH-SY5Y cells (left panel) and of SH-SY5Y cells expressing
5 wild type SOD1 or G93A-SOD1 (right panel). Cells were cultured in normal
6 growth medium for 24 hours, and then shifted to serum-free medium for 18 h.
7
8 Supernatants were concentrated as described in Materials and Methods.
9
10 Western blot analysis was done on equal volume of concentrated supernatant.
11
12 To normalize the amounts of secreted protein to the cell number, cells were
13 lysed in equivalent volumes of buffer. Western blot analysis of b-actin was
14 done on the same volume of cell extract from each sample. Data are
15 representative of three independent experiments.
16
17
18
19
20
21
22
23
24

25 **Figure 4. Analysis of the expression of genes involved in neuritogenesis in the**
26 **G93A-Sod1 mouse model.**
27

28
29 A. qPCR analysis of the expression of a subset of axon guidance genes in spinal
30 cord and brain of symptomatic *G93A-Sod1* mice. Total RNA was extracted
31 from spinal chord and brain of mice at 150 days of age. Data are presented
32 means±standard error of the mean of three technical replicates of age-matched
33 non-transgenic controls (n=3) and disease (n=4) spinal cord and brain samples.
34
35 By a 2-tailed t-test *Hgf* is considered extremely significant ($p \leq 0,0001$), *Cxcr4*
36 very significant ($p = 0.0042$), and *Sema3A* significant ($p = 0.0167$).
37
38
39
40
41
42
43 B. Time course of *Hgf* and *Cxcr4* mRNA expression in the spinal cord of *G93A-*
44 *Sod1* mice during disease progression. Total RNA was isolated from the spinal
45 cord of *G93A-SOD1*(closed circles) or age-matched non-transgenic control
46 animals (opened circles) on different days from the pre-onset till the
47 symptomatic stage (93-170 days). Expression was analyzed by RT-qPCR and
48
49
50
51
52
53
54
55
56
57
58
59
60

1
2 normalized to *Hprt1* mRNA. Standard curves represent the correlation between
3
4 delta Ct(transcript) and age. A decrease in Ct value correlates with an increase
5
6 of transcript level. Data were analyzed with a linear regression model. The
7
8 difference in slope between the two straight lines is very significant for *Cxcr4*
9
10 (r-squared = 0.911, t = 7.905, p=0.01) and extremely significant for *Hgf* (r-
11
12 squared = 0.635, t = 2.823, a p<0.001).
13

14 C. *Wasf3* and *Sept2* mRNA expression is upregulated in the spinal cord of G93A-
15
16 SOD1 mice at the early symptomatic stage. Spinal cord samples were grouped
17
18 in pre-onset phase (93, 103, and 113 days; Ntg: n=6; G93A: n=5), early
19
20 symptomatic phase (135 days; Ntg: n=2; G93A: n=2) and symptomatic phase
21
22 (145, 155, 170 days; Ntg: n=3; G93A: n=7). Each sample was analysed in
23
24 duplicates. Each bar represents the mean \pm s tandard error of each group
25
26 normalized to the mean value of the control samples at pre-onset.
27
28
29
30

31 **Figure 5. Experimental validation of the alternative internal exons identified by**
32
33 **microarray analysis.**

- 34 A. Identification of differential alternative splicing by exon array probeset-level
35
36 expression data for the entire *RPRDIA* gene in the PQ experiment. Plotted are
37
38 expression levels (y-axis) for each probeset (x-axis). Non-parallel probe set
39
40 expression levels, highlighted by a box, indicate region-dependent differential
41
42 splicing of the corresponding exon. Black line untreated; grey line: PQ-treated.
43
44
- 45 B. Exon structure of the human *RPRDIA* transcripts annotated in the Ensembl
46
47 database. Indicated are the alternative exon 8 (e8), the position of the PCR
48
49 primers, and the size of the expected products (359 bp and 968 bp).
50
51
- 52 C. RT-PCR validation of the exon array prediction for the inclusion of exon 8 in
53
54

1
2 *RPRD1A* transcripts. The indicated fragments were subcloned and sequenced to
3
4 verify their identity.
5

6 D. RT-PCR validation of the predicted ASEs for the *BINI* transcripts. The

7 indicated splice forms were subcloned and sequenced to verify their identity.
8

9
10 Left: analysis of PCR products validating alternative splicing changes. These
11 products correspond to either the inclusion or the skipping of both e14
12 (ENSE00000925812) and e16 (ENSE00000964173), and the inclusion of e7
13 (ENSE00000925822). The asterisks indicate PCR products that do not change
14 upon treatment. Right: diagrams of the relevant pre-mRNA region. Indicated are
15 the positions of the PCR primers (arrow heads), the splicing pattern, and the size
16 of the expected products (468 bp and 359 bp).
17
18
19
20
21
22
23

24 E. The bar graph represents the quantitation of the RNA splicing analysis for the

25 exon 7 (e7) of the *BINI* gene. The inclusion of exon 7 after PQ treatment and in
26 G93A-*SOD1* cells was normalized relative to that observed in the respective
27 controls (light grey bars). The dark grey bars show the average fold-increase of
28 the isoform containing exon 7; error bars indicate the standard error. The
29 asterisk represents the result of two-tailed t-test ($p < 0.05$).
30
31
32
33
34
35

36 F. Quantitation of the alternative splicing of exon 14 (e14) and exon 16 (e16) of

37 the *BINI* gene. The dark grey bars show the average fold-increase after PQ
38 treatment normalized to the untreated control (light grey bars). Error bars
39 indicate the standard error. The asterisks represent the result of two-tailed t-test
40 ($p \leq 0.001$).
41
42
43
44
45
46

47 G. Alternative splicing of *GNAOI*. The dark grey bars show the average fold

48 increase of the isoform containing exon 10 (ENSE00001322402) after PQ
49 treatment and in G93A-*SOD1* cells. Error bars indicate the standard error. The
50
51
52
53
54
55
56
57
58
59
60

1
2 asterisk represents the result of two-tailed t-test ($p \leq 0.05$).
3
4
5

6
7 Figure 6. **Experimental validation of the alternative first exons identified by**
8 **microarray analysis.**
9

- 10 A. Exon structure of the human *ABLIM1* transcripts annotated in the NCBI
11 database.
12
13
14 B. Identification of differential alternative splicing by exon array probe set-level
15 expression data for the entire *ABLIM1* gene in the paraquat (*left panel*) and the
16 *G93A-SOD1* (*right panel*) experiments. Plotted are the average signal
17 intensities (y-axis) for each probe set (x-axis). The box indicates the internal
18 first exon (exon-level probe set id: 3308001, Ensembl id: ENSE00001449337,
19 ENSE00001513698, ENSE00001449334) validated by competitive RT-PCR.
20 Black line untreated or WT-*SOD1*; red line: PQ-treated or *G93A-SOD1*.
21
22 C. RT-PCR validation of the exon array prediction for the *ABLIM1* transcript.
23 The indicated splice forms were subcloned and sequenced to verify their
24 identity. Left: analysis of PCR products validating alternative splicing
25 changes. Right: diagrams of the relevant pre-mRNA region. Indicated are: the
26 position of the PCR primers (arrow heads), the splicing pattern, and the size of
27 the expected products.
28
29 D. RT-PCR validation of the exon array prediction for three additional genes.
30 Common names of the alternatively spliced transcripts are as follows: *CHN1*,
31 chimerin 1 (GTPase-activating protein for p21-rac and a phorbol ester
32 receptor); *LMO3*, LIM domain only 3 (neuronal basic helix-loop-helix
33 protein); *NRG1*, neuregulin 1 (a signaling protein). The indicated fragments
34 were subcloned and sequenced to verify their identity. Left: analysis of PCR
35
36
37
38
39
40
41
42
43
44
45
46
47
48
49
50
51
52
53
54
55
56
57
58
59
60

1
2 products validating alternative splicing changes. Right: diagrams of the
3 relevant pre-mRNA region. Indicated are the positions of the PCR primers
4 (arrow heads), the splicing pattern, and the size of the expected products.
5
6
7

8
9 E. Confirmation of the region-specific alternative splicing pattern of CHN1 by
10 qRT-PCR. The bar graph shows the ration of the expression level of the
11 variant isoform in treated vs. untreated and WT-*SOD1* vs. G93A-*SOD1* cells.
12
13 The mRNA variant containing the first alternative exon is reduced at least 2-
14 fold upon PQ treatment.
15
16
17

18
19 F. Graphical view of the PROSITE (Swiss Institute of Bioinformatics,
20 (Gasteiger, et al., 2003) patterns predicted for the protein isoforms encoded by
21 the alternative transcripts of the *ABLIM1*, *CHN1*, *NRG1* genes. Domain
22 legend: EGF_1, EGF-like domain signature 1; EGF_3, EGF-like domain
23 profile; HP, Headpiece domain profile; IG_LIKE, Ig-like domain profile;
24
25 LIM_DOMAIN_2, LIM domain profile; RHOGAP, Rho GTPase-activating
26 proteins domain profile; SH2, Src homology 2 (SH2) domain profile;
27
28 ZF_DAG_PE_2, Zinc finger phorbol-ester/DAG-type profile.
29
30
31
32
33
34
35
36
37
38
39
40
41
42
43
44
45
46
47
48
49
50
51
52
53
54
55
56
57
58
59
60

References

- 1
2
3
4 Aerbajinai W, Ishihara T, Arahata K, Tsukahara T. 2002. Increased expression level
5
6 of the splicing variant of SIP1 in motor neuron diseases. *Int J Biochem Cell*
7
8 *Biol* 34(6):699-707.
9
- 10 [Anderson KN, Baban D, Oliver PL, Potter A, Davies KE. 2004. Expression profiling](#)
11 [in spinal muscular atrophy reveals an RNA binding protein deficit.](#)
12
13 [Neuromuscul Disord](#) 14(11):711-22.
14
- 15 [Barreau C, Paillard L, Mereau A, Osborne HB. 2006. Mammalian CELF/Bruno-like](#)
16 [RNA-binding proteins: molecular characteristics and biological functions.](#)
17
18 [Biochimie](#) 88(5):515-25.
19
- 20
21
22 Biamonti G, Caceres JF. 2009. Cellular stress and RNA splicing. *Trends Biochem Sci*
23
24 34(3):146-53.
25
- 26
27 Birney E, Stamatoyannopoulos JA, Dutta A, Guigo R, Gingeras TR, Margulies EH,
28
29 Weng Z, Snyder M, Dermitzakis ET, Thurman RE and others. 2007.
30
31 Identification and analysis of functional elements in 1% of the human genome
32
33 by the ENCODE pilot project. *Nature* 447(7146):799-816.
34
- 35
36 Boillee S, Vande Velde C, Cleveland DW. 2006. ALS: a disease of motor neurons
37
38 and their nonneuronal neighbors. *Neuron* 52(1):39-59.
39
- 40
41 Bolstad BM, Irizarry RA, Astrand M, Speed TP. 2003. A comparison of
42
43 normalization methods for high density oligonucleotide array data based on
44
45 variance and bias. *Bioinformatics* 19(2):185-93.
46
- 47
48 Breitling R, Armengaud P, Amtmann A, Herzyk P. 2004. Rank products: a simple,
49
50 yet powerful, new method to detect differentially regulated genes in replicated
51
52 microarray experiments. *FEBS Lett* 573(1-3):83-92.
53
54
55
56
57
58
59
60

- 1
2 Brockington A, Heath PR, Holden H, Kasher P, Bender FL, Claes F, Lambrechts D,
3
4 Sendtner M, Carmeliet P, Shaw PJ. 2010. Downregulation of genes with a
5
6 function in axon outgrowth and synapse formation in motor neurones of the
7
8 VEGF delta/delta mouse model of amyotrophic lateral sclerosis. *BMC*
9
10 *Genomics* 11(1):203.
11
12 Brown M, Jacobs T, Eickholt B, Ferrari G, Teo M, Monfries C, Qi RZ, Leung T, Lim
13
14 L, Hall C. 2004. Alpha2-chimaerin, cyclin-dependent Kinase 5/p35, and its
15
16 target collapsin response mediator protein-2 are essential components in
17
18 semaphorin 3A-induced growth-cone collapse. *J Neurosci* 24(41):8994-9004.
19
20 Carri MT, Ferri A, Battistoni A, Famhy L, Gabbianelli R, Poccia F, Rotilio G. 1997.
21
22 Expression of a Cu,Zn superoxide dismutase typical of familial amyotrophic
23
24 lateral sclerosis induces mitochondrial alteration and increase of cytosolic
25
26 Ca²⁺ concentration in transfected neuroblastoma SH-SY5Y cells. *FEBS Lett*
27
28 414(2):365-8.
29
30 Castello PR, Drechsel DA, Patel M. 2007. Mitochondria are a major source of
31
32 paraquat-induced reactive oxygen species production in the brain. *J Biol Chem*
33
34 282(19):14186-93.
35
36 Chalasani SH, Sabelko KA, Sunshine MJ, Littman DR, Raper JA. 2003. A
37
38 chemokine, SDF-1, reduces the effectiveness of multiple axonal repellents and
39
40 is required for normal axon pathfinding. *J Neurosci* 23(4):1360-71.
41
42 Chio A, Schymick JC, Restagno G, Scholz SW, Lombardo F, Lai SL, Mora G, Fung
43
44 HC, Britton A, Arepalli S and others. 2009. A two-stage genome-wide
45
46 association study of sporadic amyotrophic lateral sclerosis. *Hum Mol Genet*
47
48 18(8):1524-32.
49
50
51
52
53
54
55
56
57
58
59
60

1
2
3
4
5
6
7
8
9
10
11
12
13
14
15
16
17
18
19
20
21
22
23
24
25
26
27
28
29
30
31
32
33
34
35
36
37
38
39
40
41
42
43
44
45
46
47
48
49
50
51
52
53
54
55
56
57
58
59
60

[Cicchetti F, Drouin-Ouellet J, Gross RE. 2009. Environmental toxins and Parkinson's disease: what have we learned from pesticide-induced animal models? Trends Pharmacol Sci 30\(9\):475-83.](#)

Deleted: ¶

Conforti L, Adalbert R, Coleman MP. 2007. Neuronal death: where does the end begin? Trends Neurosci 30(4):159-66.

Cooper SJ, Trinklein ND, Anton ED, Nguyen L, Myers RM. 2006. Comprehensive analysis of transcriptional promoter structure and function in 1% of the human genome. Genome Res 16(1):1-10.

Cooper TA, Wan L, Dreyfuss G. 2009. RNA and disease. Cell 136(4):777-93.

Cozzolino M, Ferri A, Carri MT. 2008. Amyotrophic lateral sclerosis: from current developments in the laboratory to clinical implications. Antioxid Redox Signal 10(3):405-43.

Cozzolino M, Pesaresi MG, Amori I, Crosio C, Ferri A, Nencini M, Carri MT. 2009. Oligomerization of mutant SOD1 in mitochondria of motoneuronal cells drives mitochondrial damage and cell toxicity. Antioxid Redox Signal 11(7):1547-58.

Damiano M, Starkov AA, Petri S, Kipiani K, Kiaei M, Mattiazzi M, Flint Beal M, Manfredi G. 2006. Neural mitochondrial Ca²⁺ capacity impairment precedes the onset of motor symptoms in G93A Cu/Zn-superoxide dismutase mutant mice. J Neurochem 96(5):1349-61.

De Vos KJ, Grierson AJ, Ackerley S, Miller CC. 2008. Role of axonal transport in neurodegenerative diseases. Annu Rev Neurosci 31:151-73.

Della Beffa C, Cordero F, Calogero RA. 2008. Dissecting an alternative splicing analysis workflow for GeneChip Exon 1.0 ST Affymetrix arrays. BMC Genomics 9:571.

- 1
2 Dupuis L, de Tapia M, Rene F, Lutz-Bucher B, Gordon JW, Mercken L, Pradier L,
3
4 Loeffler JP. 2000. Differential screening of mutated SOD1 transgenic mice
5
6 reveals early up-regulation of a fast axonal transport component in spinal cord
7
8 motor neurons. *Neurobiol Dis* 7(4):274-85.
9
- 10 Edgar R, Domrachev M, Lash AE. 2002. Gene Expression Omnibus: NCBI gene
11
12 expression and hybridization array data repository. *Nucleic Acids Res*
13
14 30(1):207-10.
15
- 16 Ferri A, Cozzolino M, Crosio C, Nencini M, Casciati A, Gralla EB, Rotilio G,
17
18 Valentine JS, Carri MT. 2006. Familial ALS-superoxide dismutases associate
19
20 with mitochondria and shift their redox potentials. *Proc Natl Acad Sci U S A*
21
22 103(37):13860-5.
23
- 24 Fischer LR, Culver DG, Tennant P, Davis AA, Wang M, Castellano-Sanchez A, Khan
25
26 J, Polak MA, Glass JD. 2004. Amyotrophic lateral sclerosis is a distal
27
28 axonopathy: evidence in mice and man. *Exp Neurol* 185(2):232-40.
29
- 30 Flicek P, Aken BL, Beal K, Ballester B, Caccamo M, Chen Y, Clarke L, Coates G,
31
32 Cunningham F, Cutts T and others. 2008. Ensembl 2008. *Nucleic Acids Res*
33
34 36(Database issue):D707-14.
35
- 36 Gardina PJ, Clark TA, Shimada B, Staples MK, Yang Q, Veitch J, Schweitzer A,
37
38 Awad T, Sugnet C, Dee S and others. 2006. Alternative splicing and
39
40 differential gene expression in colon cancer detected by a whole genome exon
41
42 array. *BMC Genomics* 7:325.
43
- 44 Gasteiger E, Gattiker A, Hoogland C, Ivanyi I, Appel RD, Bairoch A. 2003. ExpASY:
45
46 The proteomics server for in-depth protein knowledge and analysis. *Nucleic*
47
48 *Acids Res* 31(13):3784-8.
49
50
51
52
53
54

- 1
2
3 Gibson GE, Starkov A, Blass JP, Ratan RR, Beal MF. 2009. Cause and consequence:
4 Mitochondrial dysfunction initiates and propagates neuronal dysfunction,
5 neuronal death and behavioral abnormalities in age-associated
6 neurodegenerative diseases. *Biochim Biophys Acta*. [1802\(1\):122-34](#)
7
8
9
10 Giger RJ, Cloutier JF, Sahay A, Prinjha RK, Levengood DV, Moore SE, Pickering S,
11 Simmons D, Rastan S, Walsh FS and others. 2000. Neuropilin-2 is required in
12 vivo for selective axon guidance responses to secreted semaphorins. *Neuron*
13 25(1):29-41.
14
15
16
17
18 Gitai Z, Yu TW, Lundquist EA, Tessier-Lavigne M, Bargmann CI. 2003. The netrin
19 receptor UNC-40/DCC stimulates axon attraction and outgrowth through
20 enabled and, in parallel, Rac and UNC-115/AbLIM. *Neuron* 37(1):53-65.
21
22
23
24 Gurney ME, Pu H, Chiu AY, Dal Canto MC, Polchow CY, Alexander DD, Caliendo
25 J, Hentati A, Kwon YW, Deng HX and others. 1994. Motor neuron
26 degeneration in mice that express a human Cu,Zn superoxide dismutase
27 mutation. *Science* 264(5166):1772-5.
28
29
30
31
32
33 [Hinman MN, Lou H. 2008. Diverse molecular functions of Hu proteins. *Cell Mol Life*](#)
34 [Sci 65\(20\):3168-81.](#)
35
36
37 Irizarry RA, Hobbs B, Collin F, Beazer-Barclay YD, Antonellis KJ, Scherf U, Speed
38 TP. 2003. Exploration, normalization, and summaries of high density
39 oligonucleotide array probe level data. *Biostatistics* 4(2):249-64.
40
41
42 Jaiswal MK, Keller BU. 2009. Cu/Zn superoxide dismutase typical for familial
43 amyotrophic lateral sclerosis increases the vulnerability of mitochondria and
44 perturbs Ca²⁺ homeostasis in SOD1G93A mice. *Mol Pharmacol* 75(3):478-
45 89.
46
47
48
49
50
51
52
53
54
55
56
57
58
59
60

- 1
2 Jaiswal MK, Zech WD, Goos M, Leutbecher C, Ferri A, Zippelius A, Carri MT, Nau
3
4 R, Keller BU. 2009. Impairment of mitochondrial calcium handling in a
5
6 mtSOD1 cell culture model of motoneuron disease. *BMC Neurosci* 10:64.
7
- 8 Jiang YM, Yamamoto M, Kobayashi Y, Yoshihara T, Liang Y, Terao S, Takeuchi H,
9
10 Ishigaki S, Katsuno M, Adachi H and others. 2005. Gene expression profile of
11
12 spinal motor neurons in sporadic amyotrophic lateral sclerosis. *Ann Neurol*
13
14 57(2):236-51.
15
- 16 Jokic N, Gonzalez de Aguilar JL, Dimou L, Lin S, Fergani A, Ruegg MA, Schwab
17
18 ME, Dupuis L, Loeffler JP. 2006. The neurite outgrowth inhibitor Nogo-A
19
20 promotes denervation in an amyotrophic lateral sclerosis model. *EMBO Rep*
21
22 7(11):1162-7.
23
- 24 Kaneko S, Iwanami A, Nakamura M, Kishino A, Kikuchi K, Shibata S, Okano HJ,
25
26 Ikegami T, Moriya A, Konishi O and others. 2006. A selective Sema3A
27
28 inhibitor enhances regenerative responses and functional recovery of the
29
30 injured spinal cord. *Nat Med* 12(12):1380-9.
31
32
- 33 Kania A, Johnson RL, Jessell TM. 2000. Coordinate roles for LIM homeobox genes
34
35 in directing the dorsoventral trajectory of motor axons in the vertebrate limb.
36
37 *Cell* 102(2):161-73.
38
- 39 Karni R, de Stanchina E, Lowe SW, Sinha R, Mu D, Krainer AR. 2007. The gene
40
41 encoding the splicing factor SF2/ASF is a proto-oncogene. *Nat Struct Mol*
42
43 *Biol* 14(3):185-93.
44
- 45 Lagier-Tourenne C, Cleveland DW. 2009. Rethinking ALS: the FUS about TDP-43.
46
47 *Cell* 136(6):1001-4.
48
- 49 Leprince C, Le Scolan E, Meunier B, Fraissier V, Brandon N, De Gunzburg J,
50
51 Camonis J. 2003. Sorting nexin 4 and amphiphysin 2, a new partnership
52
53
54
55
56
57
58
59
60

- 1
2 between endocytosis and intracellular trafficking. *J Cell Sci* 116(Pt 10):1937-
3
4 48.
5
6 Lesnick TG, Sorenson EJ, Ahlskog JE, Henley JR, Shehadeh L, Papapetropoulos S,
7
8 Maraganore DM. 2008. Beyond Parkinson disease: amyotrophic lateral
9
10 sclerosis and the axon guidance pathway. *PLoS One* 3(1):e1449.
11
12 Licatalosi DD, Darnell RB. 2006. Splicing regulation in neurologic disease. *Neuron*
13
14 52(1):93-101.
15
16 Lin H, Zhai J, Schlaepfer WW. 2005. RNA-binding protein is involved in aggregation
17
18 of light neurofilament protein and is implicated in the pathogenesis of motor
19
20 neuron degeneration. *Hum Mol Genet* 14(23):3643-59.
21
22 Magrane J, Manfredi G. 2009. Mitochondrial function, morphology, and axonal
23
24 transport in amyotrophic lateral sclerosis. *Antioxid Redox Signal*. [11\(7\):1615-](#)
25
26 [26](#).
27
28
29 Maracchioni A, Totaro A, Angelini DF, Di Penta A, Bernardi G, Carri MT, Achsel T.
30
31 2007. Mitochondrial damage modulates alternative splicing in neuronal cells:
32
33 implications for neurodegeneration. *J Neurochem* 100(1):142-53.
34
35 Mattiazzi M, D'Aurelio M, Gajewski CD, Martushova K, Kiaei M, Beal MF,
36
37 Manfredi G. 2002. Mutated human SOD1 causes dysfunction of oxidative
38
39 phosphorylation in mitochondria of transgenic mice. *J Biol Chem*
40
41 277(33):29626-33.
42
43 Munch C, Ebstein M, Seefried U, Zhu B, Stamm S, Landwehrmeyer GB, Ludolph
44
45 AC, Schwalenstocker B, Meyer T. 2002. Alternative splicing of the 5'-
46
47 sequences of the mouse EAAT2 glutamate transporter and expression in a
48
49 transgenic model for amyotrophic lateral sclerosis. *J Neurochem* 82(3):594-
50
51 603.
52
53
54
55
56
57
58
59
60

- 1
2
3
4
5
6
7
8
9
10
11
12
13
14
15
16
17
18
19
20
21
22
23
24
25
26
27
28
29
30
31
32
33
34
35
36
37
38
39
40
41
42
43
44
45
46
47
48
49
50
51
52
53
54
55
56
57
58
59
60
- Nguyen KT, Garcia-Chacon LE, Barrett JN, Barrett EF, David G. 2009. The Psi(m) depolarization that accompanies mitochondrial Ca²⁺ uptake is greater in mutant SOD1 than in wild-type mouse motor terminals. *Proc Natl Acad Sci U S A* 106(6):2007-11.
- Nicot AS, Toussaint A, Tosch V, Kretz C, Wallgren-Pettersson C, Iwarsson E, Kingston H, Garnier JM, Biancalana V, Oldfors A and others. 2007. Mutations in amphiphysin 2 (BIN1) disrupt interaction with dynamin 2 and cause autosomal recessive centronuclear myopathy. *Nat Genet* 39(9):1134-9.
- O'Donnell M, Chance RK, Bashaw GJ. 2009. Axon growth and guidance: receptor regulation and signal transduction. *Annu Rev Neurosci* 32:383-412.
- Okoniewski MJ, Yates T, Dibben S, Miller CJ. 2007. An annotation infrastructure for the analysis and interpretation of Affymetrix exon array data. *Genome Biol* 8(5):R79.
- Olsson PA, Bornhauser BC, Korhonen L, Lindholm D. 2000. Neuronal expression of the ERM-like protein MIR in rat brain and its localization to human chromosome 6. *Biochem Biophys Res Commun* 279(3):879-83.
- Olsson PA, Korhonen L, Mercer EA, Lindholm D. 1999. MIR is a novel ERM-like protein that interacts with myosin regulatory light chain and inhibits neurite outgrowth. *J Biol Chem* 274(51):36288-92.
- [Pan Q, Shai O, Misquitta C, Zhang W, Saltzman AL, Mohammad N, Babak T, Siu H, Hughes TR, Morris QD and others. 2004. Revealing global regulatory features of mammalian alternative splicing using a quantitative microarray platform. *Mol Cell* 16\(6\):929-41.](#)

- 1
2
3 Pant S, Sharma M, Patel K, Caplan S, Carr CM, Grant BD. 2009. AMPH-
4 1/Amphiphysin/Bin1 functions with RME-1/Ehd1 in endocytic recycling. *Nat*
5 *Cell Biol* 11(12):1399-410.
6
7
8 Pantelidou M, Zographos SE, Lederer CW, Kyriakides T, Pfaffl MW, Santama N.
9
10 2007. Differential expression of molecular motors in the motor cortex of
11 sporadic ALS. *Neurobiol Dis* 26(3):577-89.
12
13
14 Perlson E, Jeong GB, Ross JL, Dixit R, Wallace KE, Kalb RG, Holzbaur EL. 2009. A
15 switch in retrograde signaling from survival to stress in rapid-onset
16 neurodegeneration. *J Neurosci* 29(31):9903-17.
17
18
19
20 Pizzasegola C, Caron I, Daleno C, Ronchi A, Minoia C, Carri MT, Bendotti C. 2009.
21 Treatment with lithium carbonate does not improve disease progression in two
22 different strains of SOD1 mutant mice. *Amyotroph Lateral Scler* 10(4):221-8.
23
24
25
26 Polleux F, Ince-Dunn G, Ghosh A. 2007. Transcriptional regulation of vertebrate
27 axon guidance and synapse formation. *Nat Rev Neurosci* 8(5):331-40.
28
29
30
31 Pun S, Santos AF, Saxena S, Xu L, Caroni P. 2006. Selective vulnerability and
32 pruning of phasic motoneuron axons in motoneuron disease alleviated by
33 CNTF. *Nat Neurosci* 9(3):408-19.
34
35
36
37 Robertson J, Doroudchi MM, Nguyen MD, Durham HD, Strong MJ, Shaw G, Julien
38 JP, Mushynski WE. 2003. A neurotoxic peripherin splice variant in a mouse
39 model of ALS. *J Cell Biol* 160(6):939-49.
40
41
42
43 Robinow S, Campos AR, Yao KM, White K. 1988. The elav gene product of
44 Drosophila, required in neurons, has three RNP consensus motifs. *Science*
45 242(4885):1570-2.
46
47 Rothstein JD. 2009. Current hypotheses for the underlying biology of amyotrophic
48 lateral sclerosis. *Ann Neurol* 65 Suppl 1:S3-9.
49
50
51
52
53
54

- 1
2 Sanges R, Cordero F, Calogero RA. 2007. oneChannelGUI: a graphical interface to
3
4 Bioconductor tools, designed for life scientists who are not familiar with R
5
6 language. *Bioinformatics* 23(24):3406-8.
7
8 Schmidt ER, Pasterkamp RJ, van den Berg LH. 2009. Axon guidance proteins: novel
9
10 therapeutic targets for ALS? *Prog Neurobiol* 88(4):286-301.
11
12 Shi L, Fu WY, Hung KW, Porchetta C, Hall C, Fu AK, Ip NY. 2007. Alpha2-
13
14 chimaerin interacts with EphA4 and regulates EphA4-dependent growth cone
15
16 collapse. *Proc Natl Acad Sci U S A* 104(41):16347-52.
17
18 Shi P, Gal J, Kwinter DM, Liu X, Zhu H. 2010. Mitochondrial dysfunction in
19
20 amyotrophic lateral sclerosis. *Biochim Biophys Acta* 1802(1):45-51.
21
22 Smyth GK. 2004. Linear models and empirical bayes methods for assessing
23
24 differential expression in microarray experiments. *Stat Appl Genet Mol Biol*
25
26 3:Article3.
27
28 Strom AL, Gal J, Shi P, Kasarskis EJ, Hayward LJ, Zhu H. 2008. Retrograde axonal
29
30 transport and motor neuron disease. *J Neurochem* 106(2):495-505.
31
32 Strong MJ. 2009. The evidence for altered RNA metabolism in amyotrophic lateral
33
34 sclerosis (ALS). *J Neurol Sci* 288(1-2):1-12.
35
36 Struckhoff EC, Lundquist EA. 2003. The actin-binding protein UNC-115 is an
37
38 effector of Rac signaling during axon pathfinding in *C. elegans*. *Development*
39
40 130(4):693-704.
41
42 Stumm R, Hollt V. 2007. CXC chemokine receptor 4 regulates neuronal migration
43
44 and axonal pathfinding in the developing nervous system: implications for
45
46 neuronal regeneration in the adult brain. *J Mol Endocrinol* 38(3):377-82.
47
48 Sugimori M, Nagao M, Bertrand N, Parras CM, Guillemot F, Nakafuku M. 2007.
49
50 Combinatorial actions of patterning and HLH transcription factors in the
51
52
53
54

- 1
2 spatiotemporal control of neurogenesis and gliogenesis in the developing
3 spinal cord. *Development* 134(8):1617-29.
- 4
5
6 Takei K, Slepnev VI, Haucke V, De Camilli P. 1999. Functional partnership between
7
8 amphiphysin and dynamin in clathrin-mediated endocytosis. *Nat Cell Biol*
9
10 1(1):33-9.
- 11
12 Tomiyama M, Rodriguez-Puertas R, Cortes R, Pazos A, Palacios JM, Mengod G.
13
14 2002. Flip and flop splice variants of AMPA receptor subunits in the spinal
15
16 cord of amyotrophic lateral sclerosis. *Synapse* 45(4):245-9.
- 17
18 Volkening K, Leystra-Lantz C, Strong MJ. 2009. Human low molecular weight
19
20 neurofilament (NFL) mRNA interacts with a predicted p190RhoGEF
21
22 homologue (RGNEF) in humans. *Amyotroph Lateral Scler*:1-7.
- 23
24 Westfall PH YS. 1993. Resampling-based multiple testing: examples and Materials
25
26 and Methods for p-value adjustment. New York: John Wiley & Sons.
- 27
28 Wolman MA, Liu Y, Tawarayama H, Shoji W, Halloran MC. 2004. Repulsion and
29
30 attraction of axons by semaphorin3D are mediated by different neuropilins in
31
32 vivo. *J Neurosci* 24(39):8428-35.
- 33
34 Yamamoto ML, Clark TA, Gee SL, Kang JA, Schweitzer AC, Wickrema A, Conboy
35
36 JG. 2009. Alternative pre-mRNA splicing switches modulate gene expression
37
38 in late erythropoiesis. *Blood* 113(14):3363-70.
- 39
40 Yates T, Okoniewski MJ, Miller CJ. 2008. X:Map: annotation and visualization of
41
42 genome structure for Affymetrix exon array analysis. *Nucleic Acids Res*
43
44 36(Database issue):D780-6.
- 45
46
47 Yonekawa Y, Harada A, Okada Y, Funakoshi T, Kanai Y, Takei Y, Terada S, Noda
48
49 T, Hirokawa N. 1998. Defect in synaptic vesicle precursor transport and
50
51
52
53
54
55
56
57
58
59
60

1
2 neuronal cell death in KIF1A motor protein-deficient mice. *J Cell Biol*
3
4 141(2):431-41.
5

6 Yoo S, van Niekerk EA, Merianda TT, Twiss JL. 2009. Dynamics of axonal mRNA
7
8 transport and implications for peripheral nerve regeneration. *Exp Neurol.*
9
10 [223\(1\):19-27.](#)
11

12 Zou YR, Kottmann AH, Kuroda M, Taniuchi I, Littman DR. 1998. Function of the
13
14 chemokine receptor CXCR4 in haematopoiesis and in cerebellar development.
15
16 *Nature* 393(6685):595-9.
17

18
19
20
21
22
23
24
25
26
27
28
29
30
31
32
33
34
35
36
37
38
39
40
41
42
43
44
45
46
47
48
49
50
51
52
53
54
55
56
57
58
59
60

For Peer Review

Tables

Table 1. **Molecular and Cellular Functions affected by PQ treatment.**

Name	p-value	Molecules
Cellular Growth and Proliferation	1.33E-18 - 1.01E-03	435
Cell Death	6.28E-17 - 1.03E-03	368
Cell Cycle	1.62E-15 - 9.86E-04	213
Cellular Development	6.75E-12 - 1.01E-03	312
Cellular Movement	4.66E-09 - 1.02E-03	240

Table 2. **Top Canonical Pathways affected by PQ treatment.**

Name	p-value	Ratio
p53 Signaling	6.77E-04	22/87
Circadian Rhythm Signaling	1.43E-03	10/32
Hepatic Fibrosis / Hepatic Stellate Cell Activation	3.02E-03	22/131
Neurotrophin/TRK Signaling	3.24E-03	13/73
NRF2-mediated Oxidative Stress Response	3.37E-03	29/180

Table 3. **Functions affected by the expression of the SOD1(G93A) protein.**

Name	p-value	Molecules
Cellular Movement	6.30E-09 - 1.13E-02	40
Cellular Assembly and Organization	9.44E-07 - 1.13E-02	25
Cell Cellular growth and Proliferation	2.72E-06 - 1.18E-02	57
Nervous System Development and Function	6.30E-09 - 1.18E-02	49
Genetic Disorders	1.78E-07 - 1.13E-02	67
Neurological Diseases	1.78E-07 - 1.13E-02	46
Psychological Diseases	1.78E-07 - 5.87E-03	20

Table 4. **Genes related to the “Nervous System Differentiation and Function” Category**

SYMBOL	DESCRIPTION	Function annotation
<i>ADORA2A</i>	adenosine A2a receptor	growth of neuritis, synaptic transmission
<i>APBA1</i>	EPH receptor A6	exocytosis of synaptic vesicles
<i>ASCL1</i>	achaete-scute complex homolog 1 (Drosophila)	neurogenesis
<i>BMP7</i>	bone morphogenetic protein 7	neurogenesis
<i>BVES</i>	blood vessel epicardial substance	regeneration of satellite cells
<i>C4ORF6</i>	chromosome 4 open reading frame 6	neurogenesis
<i>CABLES1</i>	Cdk5 and Abl enzyme substrate 1	neurogenesis
<i>CDON</i>	Cdon homolog (mouse)	differentiation of neurons

1			
2			
3	<i>CHRD1</i>	chordin-like 1	differentiation of
4			neurons
5	<i>CHRM2</i>	cholinergic receptor, muscarinic 2, cardiac	neurogenesis
6	<i>CLU</i>	clusterin	morphogenesis of
7			neurites
8			neurogenesis
9	<i>CNTN4</i>	contactin 4	neurogenesis
10	<i>DLX5</i>	distal-less homeobox 5	neurogenesis
11	<i>DPYSL5</i>	dihydropyrimidinase-like 5	neurogenesis
12	<i>ELAVL2</i>	ELAV (embryonic lethal, abnormal vision, Drosophila)-like 2 (Hu antigen B)	differentiation of
13			neurons
14	<i>GATA2</i>	GATA binding protein 2	differentiation of
15			neurons
16			neurogenesis
17	<i>GJA1</i>	gap junction protein, alpha 1	neurogenesis
18	<i>GRM7</i>	glutamate receptor, metabotropic 7	
19	<i>HEY1</i>	hairy/enhancer-of-split related with YRPW motif 1	neurogenesis
20			
21	<i>INHBA</i>	inhibin, beta A	survival of nervous
22			tissue
23			growth of neurites
24	<i>KIT</i>	kit oncogene	differentiation of
25	<i>LIFR</i>	leukemia inhibitory factor receptor alpha	neurons
26			neurogenesis
27	<i>MPPED2</i>	metallophosphoesterase domain containing 2	neurogenesis
28			
29	<i>NMU</i>	neuromedin U	synaptic transmission
30	<i>NNAT</i>	neuronatin	development of
31			nervous system
32	<i>NQO1</i>	NAD(P)H dehydrogenase, quinone 1	synaptic transmission
33	<i>NTRK1</i>	neurotrophic tyrosine kinase, receptor, type 1	neurogenesis, survival of nervous
34			tissue
35	<i>PBX1</i>	pre B-cell leukemia transcription factor 1	differentiation of
36			neurons
37			neurogenesis
38	<i>PLXNA4</i>	plexin A4	growth of neurites
39	<i>PTPRM</i>	protein tyrosine phosphatase, receptor type, M	
40			neurogenesis
41	<i>SEMA3D</i>	sema domain, immunoglobulin domain (Ig), short basic domain, secreted, (semaphorin) 3D	neurogenesis
42			
43	<i>SERPINI1</i>	serpin peptidase inhibitor, clade I (neuroserpin), member 1	development of
44			nervous system
45	<i>SERPINE2</i>	serine (or cysteine) peptidase inhibitor, clade I, member 2	integration of
46			sensorimotor cortex
47	<i>SIX3</i>	sine oculis-related homeobox 3 homolog (Drosophila)	generation of
48			neurons
49	<i>ST8SIA2</i>	ST8 alpha-N-acetyl-neuraminide alpha-2,8- sialyltransferase 2 [Mus musculus]	neurogenesis
50			
51	<i>SYT2</i>	synaptotagmin II	exocytosis of
52			synaptic vesicles
53			
54			
55			
56			
57			
58			
59			
60			

Table 5. **Molecular and Cellular Functions affected by putative ASEs in paraquat-treated SH-SY5Y cells.**

Name	p-value	Molecules
Cell Death	1.69E-18 - 1.81E-03	126
Cellular Growth and Proliferation	1.25E-15 - 1.79E-03	137
Cell Cycle	1.09E-13 - 1.90E-03	77
Cellular Development	1.21E-12 - 1.67E-03	67
Cellular Movement	2.08E-09 - 2.17E-04	90

Table 6. **Top Canonical Pathways affected by putative ASEs in SOD1(G93A) SH-SY5Y cells.**

Name	p-value	Ratio
Calcium Signaling	1.81E-03	7/206
cAMP-mediated Signaling	3.65E-03	6/162
G-Protein Coupled Receptor Signaling	3.89E-03	7/217
Neuropathic Pain Signaling in Dorsal Horn Neurons	1.49E-02	4/104
Cell Cycle:G1/S Checkpoint Regulation	1.56E-02	3/59

1
2
3
4
5
6
7
8
9
10
11
12
13
14
15
16
17
18
19
20
21
22
23
24
25
26
27
28
29
30
31
32
33
34
35
36
37
38
39
40
41
42
43
44
45
46
47
48
49
50
51
52
53
54
55
56
57
58
59
60

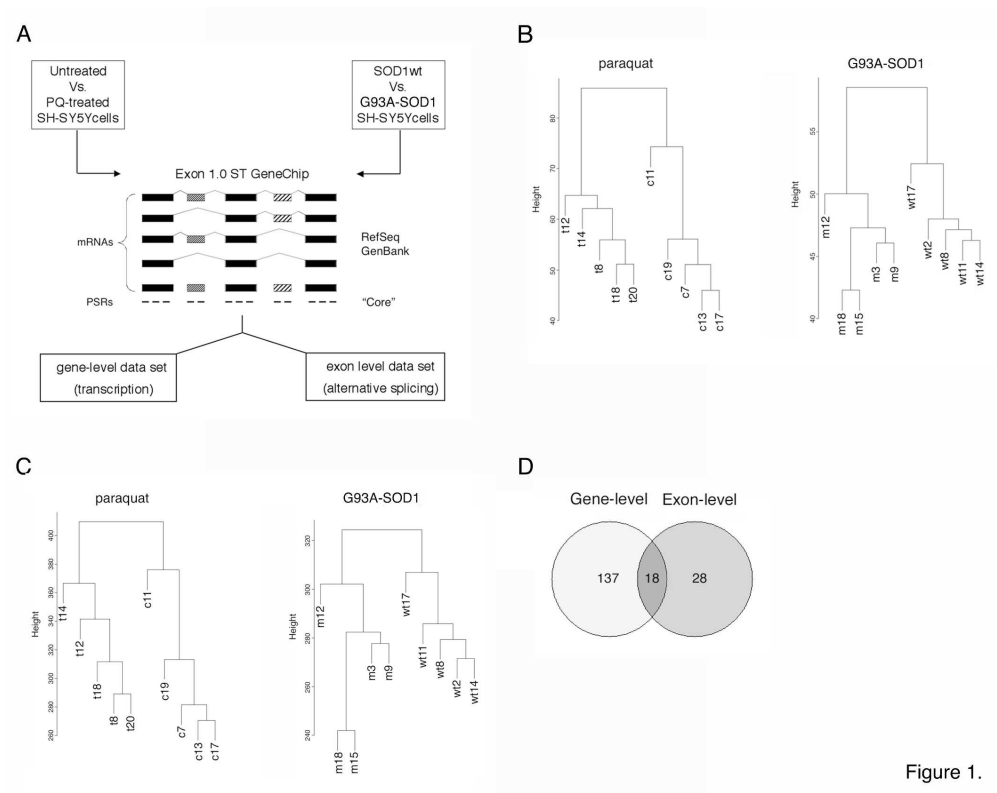


Figure 1.

Whole genome, splicing-sensitive microarray analysis of the cellular response to mitochondrial dysfunction.
180x141mm (600 x 600 DPI)

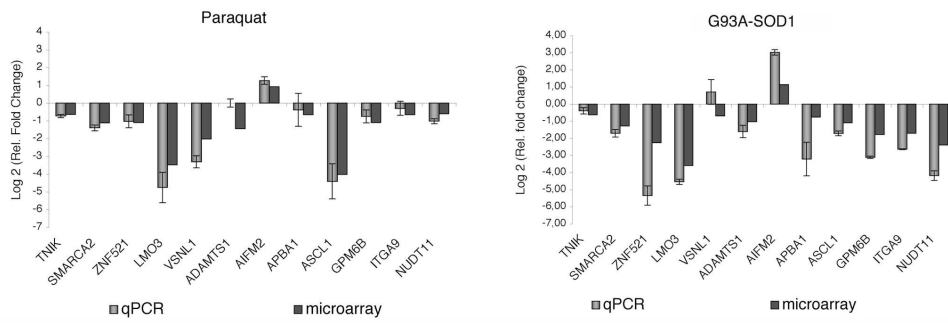


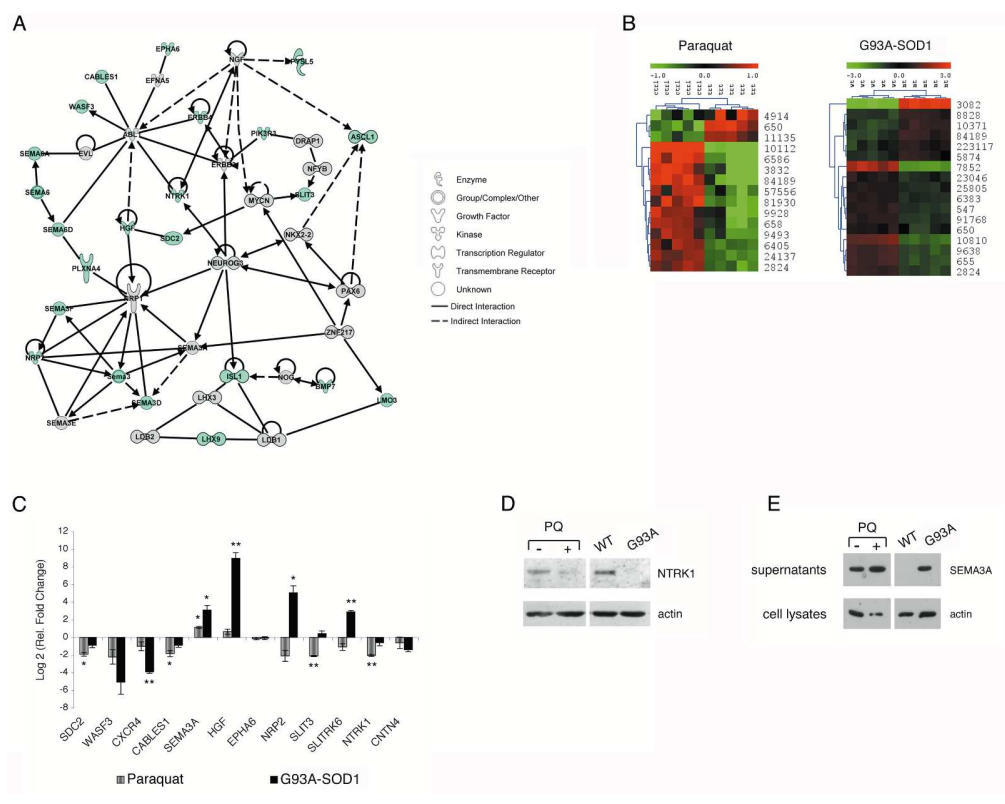
Figure 2.

Experimental validation of the gene-level microarray data in SH-SY5Y cells.
180x62mm (600 x 600 DPI)

Peer Review

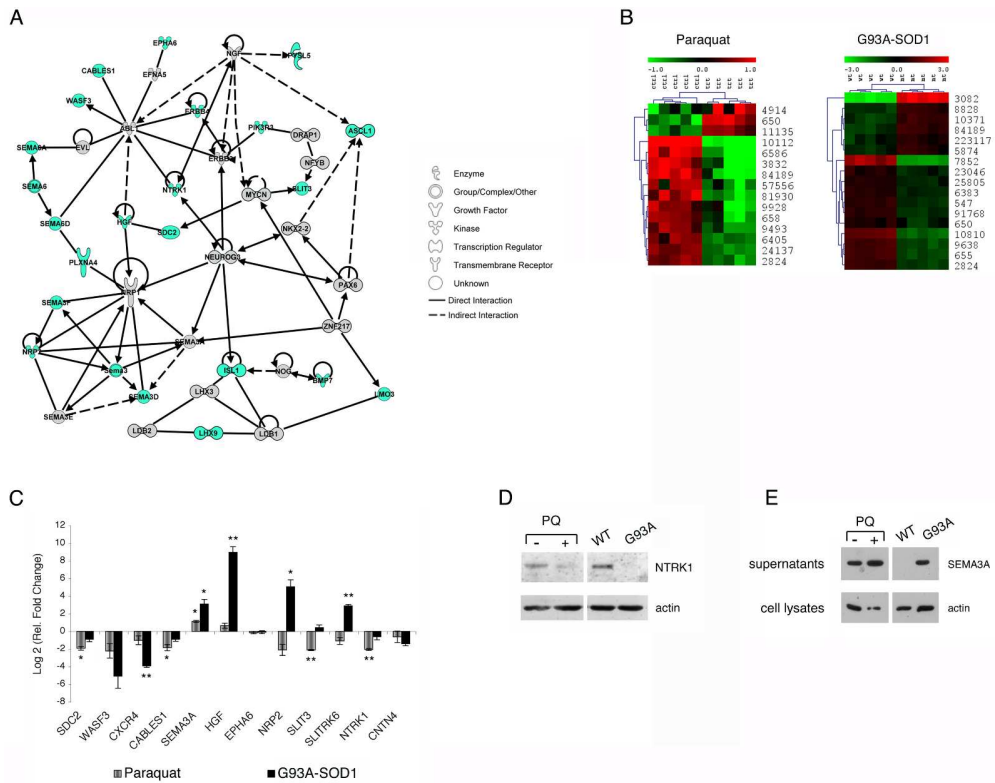
1
2
3
4
5
6
7
8
9
10
11
12
13
14
15
16
17
18
19
20
21
22
23
24
25
26
27
28
29
30
31
32
33
34
35
36
37
38
39
40
41
42
43
44
45
46
47
48
49
50
51
52
53
54
55
56
57
58
59
60

1
2
3
4
5
6
7
8
9
10
11
12
13
14
15
16
17
18
19
20
21
22
23
24
25
26
27
28
29
30
31
32
33
34
35
36
37
38
39
40
41
42
43
44
45
46
47
48
49
50
51
52
53
54
55
56
57
58
59
60



Mitochondrial dysfunction alters expression and splicing of genes involved in axon growth and guidance.
270x211mm (600 x 600 DPI)

view



Mitochondrial dysfunction alters expression and splicing of genes involved in axon growth and guidance.

270x211mm (600 x 600 DPI)

1
2
3
4
5
6
7
8
9
10
11
12
13
14
15
16
17
18
19
20
21
22
23
24
25
26
27
28
29
30
31
32
33
34
35
36
37
38
39
40
41
42
43
44
45
46
47
48
49
50
51
52
53
54
55
56
57
58
59
60

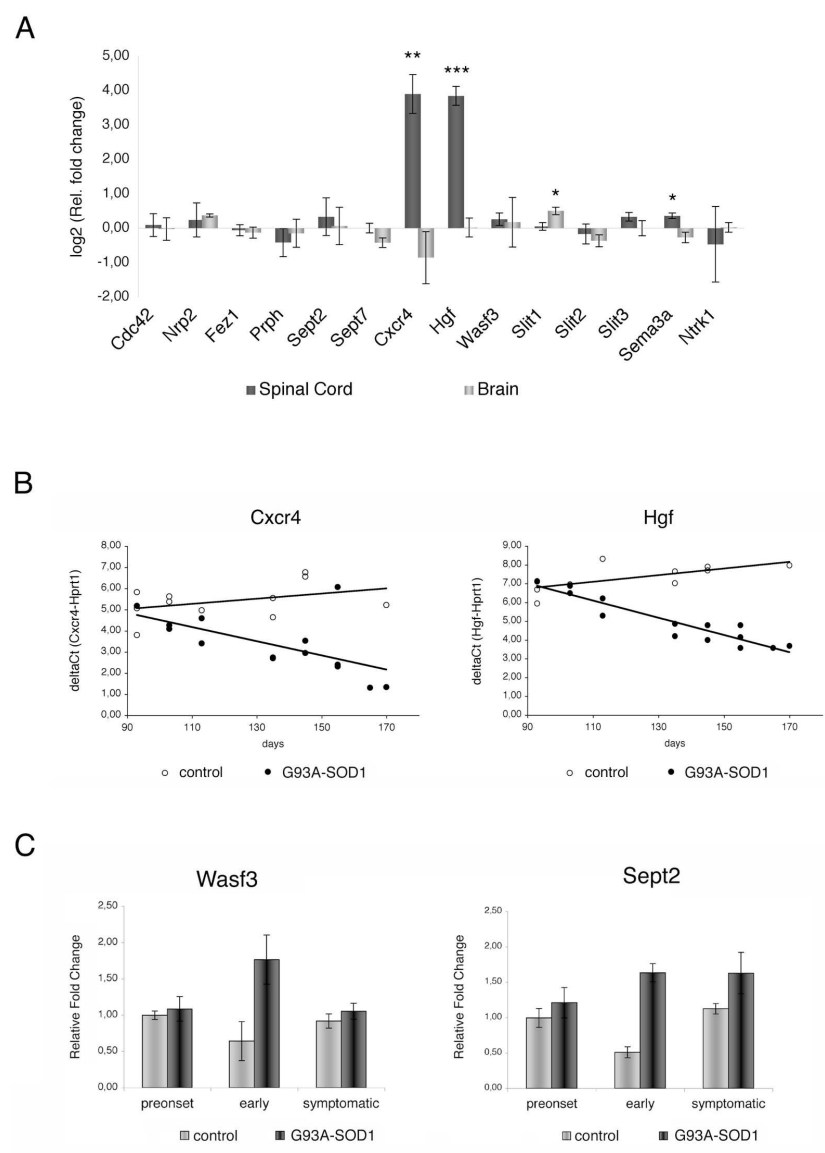


Figure 4.

Analysis of the expression of genes involved in neurogenesis in the G93A-Sod1 mouse model.
135x195mm (600 x 600 DPI)

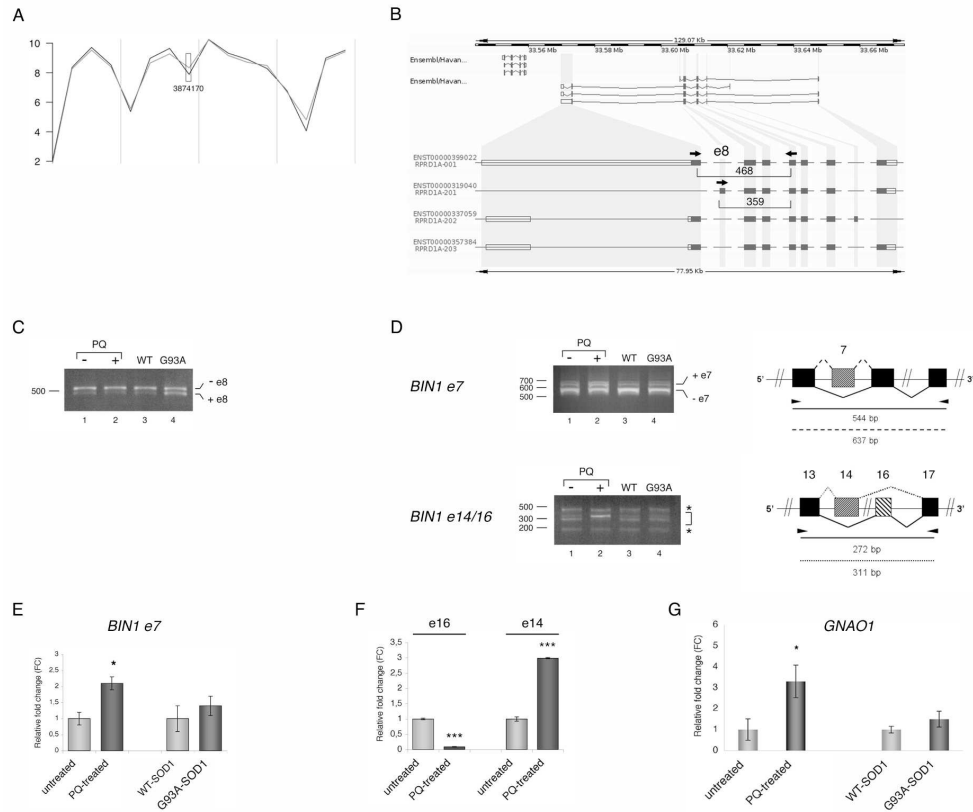


Figure 5

Experimental validation of the alternative internal exons identified by microarray analysis.
240x209mm (600 x 600 DPI)

1
2
3
4
5
6
7
8
9
10
11
12
13
14
15
16
17
18
19
20
21
22
23
24
25
26
27
28
29
30
31
32
33
34
35
36
37
38
39
40
41
42
43
44
45
46
47
48
49
50
51
52
53
54
55
56
57
58
59
60

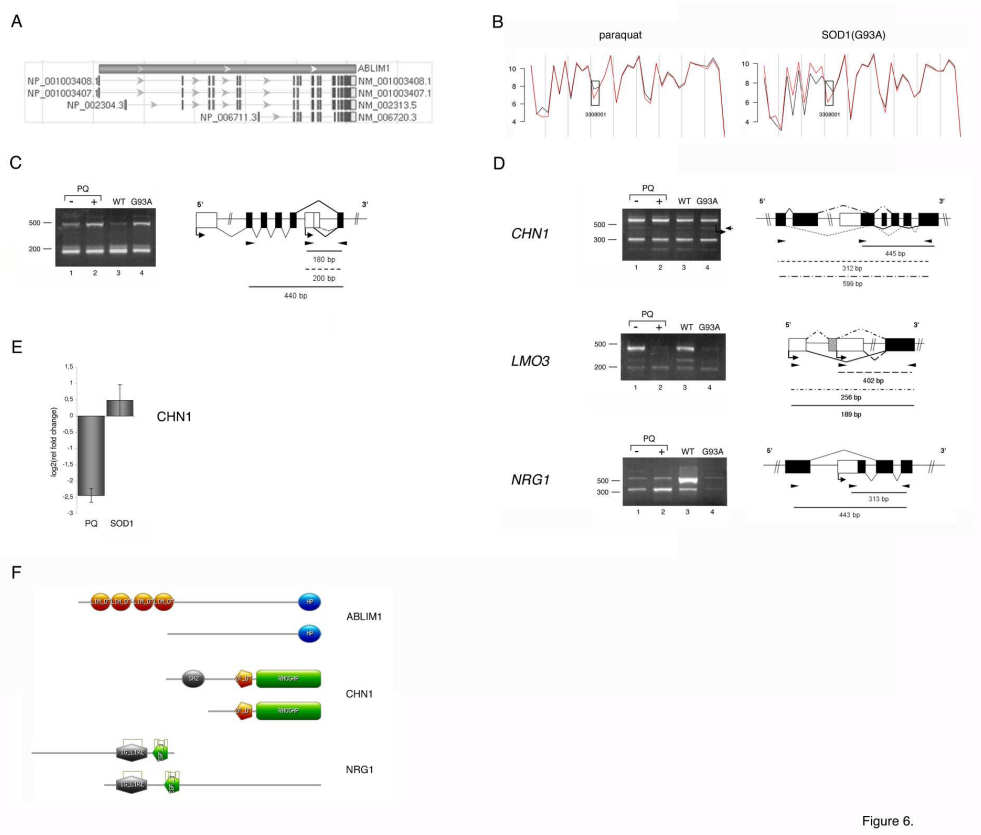


Figure 6.

Experimental validation of the alternative first exons identified by microarray analysis.
323x269mm (600 x 600 DPI)

Supporting Results

PQ treatment inhibits cell proliferation and modifies alternative pre-mRNA splicing in SH-SY5Y neuroblastoma cells

PQ is a neurotoxic herbicide that induces Parkinsonian features in animal models (for review see (Cicchetti, et al., 2009).). The chemical structure of PQ is similar to the known dopaminergic neurotoxin, N-methyl-4-phenylpyridinium ion (MPP+), the active metabolite of MPTP. Thus, it belongs to the class of redox cycling compounds capable of inducing mitochondrial damage, increasing reactive oxygen species (ROS) production and oxidative stress (Birney, et al., 2007; Castello, et al., 2007).

Concentration–response time course studies were conducted to determine an effective range for PQ upon SH-SY5Y cell proliferation. We used the MTT assay, which is mostly based on the activity of a mitochondrial dehydrogenase and therefore is largely used as a measure of mitochondrial activity. Based on the results shown in Figure S1A, we decided to perform subsequent experiments with cells exposed to 0.75 mM PQ for 18 h.

We next evaluated alternative splicing changes in these conditions. We assayed the AS pattern of *APAF1*, *BCL2L1* (BCL-X), *CASP2*, and *CASP9* (Supp. Figure S1B) that we had described in (Maracchioni, et al., 2007). Consistent with our previous data, even a treatment with lower PQ concentration and for a shorter incubation time induced a change in the alternative splicing pattern of *APAF1*, *CASP9*, and *SMN1* but not of *BCL2L1* (Supp. Figure S1C).

Deleted: and *SMN1*

Experimental validation of the differential expression data for the PQ experiment

Pathway analysis of microarray data identified *Cellular Growth and Proliferation*, *Cell Death*, and *Cell Cycle* as the biological functions that are most affected by PQ.

1
2 Thus, we first characterized the cell cycle distribution of PQ-treated cells. Flow-
3 cytometric analyses of sub-confluent, treated cells showed an increase in the G1- and
4 a decrease in the S-phase populations when compared to untreated control cells
5 (Figure S1A). This observation was consistent with the downregulation of cyclin A2
6 (*CCNA2*) and cyclin E2 (*CCNE2*) required for S/G2 progression, and of cyclin B
7 (*CCNB1*), required for G2/M transition, as well as with the upregulation of *CDKN3*, a
8 CDK2-phosphatase, and of p21 (*CDKN1B*), as detected by microarray analysis (Supp.
9 Table S1). Western blot analysis confirmed the downregulation of cyclin A and cyclin
10 B (Supp. Figure S1B). In addition, in treated cells we detected the presence of a
11 subG1 population indicating that some cell death occurred upon incubation with PQ
12 (data not shown). The induction of apoptosis was confirmed by Terminal
13 deoxynucleotidyl transferase dUTP nick end-labeling (TUNEL) assays (Supp. Figure
14 S1C). While a very low population was found in region 2 in the untreated control
15 samples, treated cells exhibited a TUNEL-positive fraction of ~20 %. Induction of
16 apoptosis in a subset of the cells was further supported by the proteolytic cleavage of
17 PARP a known caspase 1 substrate, observed by Western blotting (Supp. Figure
18 S1D).

38 **Material and Methods**

39 *Assessment of cell viability*

40
41 Cell viability was assessed with the MTT colorimetric assay. The assay is based on
42 the determination of the mitochondrial dehydrogenase activity that reduces 3-(4,5-
43 dimethylthiazol-2-yl)-2,5-diphenyl-tetrazolium bromide (MTT, Sigma-Aldrich). At
44 day 0, SH-SY5Y cells were plated at a density of 5×10^4 viable cells per well in 96-
45 well plates. The next day, cells were incubated for 24 h at 37°C in the presence of
46
47
48
49
50
51
52
53
54

1
2 different concentrations of PQ, or for different times in the presence of 0.75mM of
3
4 PQ. Cells were then exposed to an MTT-containing solution (1 mg/ml in PBS) for 4 h
5
6 at 37°C and subsequently treated with SDS in dimethylformamide o.n. Absorbance
7
8 was read at 550 and 655 nm with a Multiscan EX (Thermo Fisher Scientific Inc.).
9
10 Cytotoxicity was evaluated as percentage of the control untreated with PQ.
11
12

13 14 *Cell cycle analysis*

15
16 SH-SY5Y neuroblastoma cells were seeded at 1,2x10⁶ cells per well in 60mm dish,
17
18 and the day after were treated with 0,75mM of PQ for 18 hours. Then untreated and
19
20 treated cells, both attached and detached populations, were collected and fixed in 70%
21
22 ethanol in PBS and kept at 4°C before staining. Fixed cells were then washed with
23
24 cold PBS and resuspended in 1 mL of a solution containing 10 ug/ml of propidium
25
26 iodide (PI) in PBS and 7 µl RNase 3 mg/ml in water, and stained overnight at 4°C in
27
28 the dark. DNA analysis was done on at least 30000 cells for each sample by the
29
30 FACSCalibur (BD Biosciences - CA USA) and the data were analyzed using
31
32 ModFIT LTsoftware (Verity Software House - ME USA). Experiment was performed
33
34 in triplicate.
35
36

37 38 *TUNEL assay*

39
40 Apoptosis was measured using the TUNEL assay kit (Roche Diagnostics, Basel,
41
42 Switzerland) following the manufacturers' instruction for dual parameter flow
43
44 cytometry. Analysis was performed on a FACSCalibur (BD Biosciences – CA USA)
45
46 and the data were analyzed using Summit 4.3 software (Coulter - CA USA).
47
48
49
50
51
52
53
54

Immunoblotting

1.5x10⁶ cells were plated on p60mm Petri dishes. After treatment with paraquat, cells were rinsed in ice cold PBS and lysed in 150 μ l low salt buffer (10 mM Hepes pH 7.4, 42 mM KCl, 5mM MgCl₂, 0.5% CHAPS, 1mM DTT, 1mM PMSF, 1 μ g/ml leupeptin). After centrifugation at 20000g, nuclei were resuspended in 50 μ l high salt buffer (50mM Tris-HCl pH 7.5, 400mM NaCl, 1mM EDTA, 1% Triton X-100, 0.5% NP-40, 10% glycerol, 2mM DTT, 1mM PMSF, protease inhibitor cocktail. After 30' on ice, lysates were centrifuged at 20000g, supernatants were collected and analysed as nuclear fractions in Western blot with antibodies anti-cleaved PARP1 (Cell Signal) and anti-LaminB (Santa Cruz).

For the analysis of cyclin expression cell monolayers were washed twice with ice cold PBS and lysed on the tissue culture dish by addition of ice-cold lysis buffer (50mM Tris-HCl, pH 7.5, 150mM NaCl, and 1% NP-40, and complete protease inhibitor cocktail (Roche Diagnostics). Anti-cyclin A, and anti-cyclin B, were from BD Biosciences, (Pharmingen).

Quality control for RNA and Arrays

RNA quantity was assessed by Ribogreen (Invitrogen). Total RNA integrity was assessed using a Bioanalyzer (Agilent) and the RNA Integrity Number (RIN) was calculated. RIN values ranged from 8.7 to 10 with a media of 9.6

For target preparation 1.5 μ g of total RNA and the GeneChip WT cDNA Amplification kit (Affymetrix) were used. Amounts of ssDNA obtained ranged from 7 to 10 μ g with a media of 8.8 μ g. ssDNA before and following fragmentation was analysed using a Bioanalyzer (Agilent). Typical ssDNA fragments have a size range from 40-70 nt.

1
2
3
4
5
6
7
8
9
10
11
12
13
Hybridization to the Standard array: Fragmented ssDNAs were hybridized to the
standard arrays for 17 hours at 45°C; the arrays were then washed and stained using the
fluidics station and then scanned using GeneChip Scanner 3000. The images were
analyzed using Command Console and comparison analyses were carried out according to
the instructions provided by Affymetrix. Standard array quality controls are shown in
Supp. Figures S3-S6.

14
15
16
17
18
19
20
21
22
23
24
25
26
27
28
29
30
31
32
33
34
35
36
37
38
39
40
41
42
43
44
45
46
47
48
49
50
51
52
53
54
55
56
57
58
59
60
The “negative control”, “positive control” and “all probe set” metrics are useful in
understanding the overall quality of the data from each chip. Metrics based on these
categories will reflect the quality of the whole experiment (RNA, target prep, chip,
hybridization, scanning, and gridding) and the nature of the data being used in downstream
statistical analysis.

Supp. Figures and Tables

Deleted: ¶

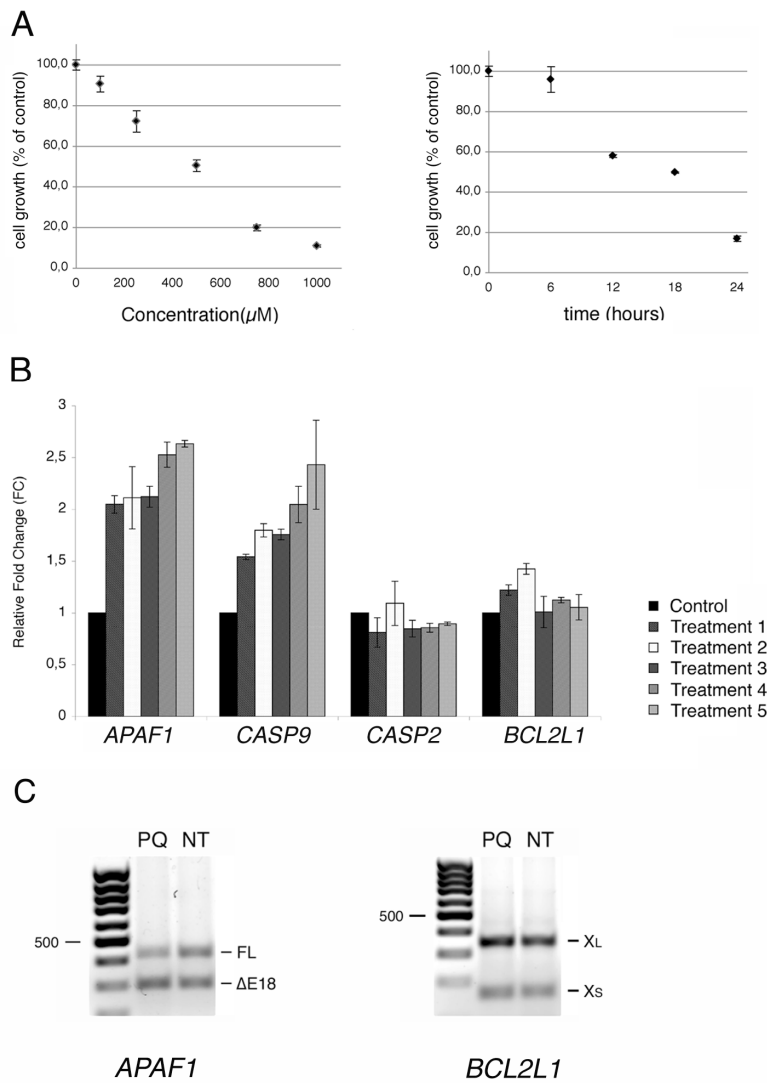


Figure S1

Figure S1. Treatment with paraquat inhibits cell proliferation and modifies alternative pre-mRNA splicing in SH-SY5Y neuroblastoma cells.

A. Effect of PQ on cell growth. Dose- (left panel) and time- (right panel) dependent effect of PQ on SH-SY5Y cells. Exponentially dividing cells were treated with increasing concentrations of PQ for 24 h, or with 0,75 mM PQ for

1
2 different times. Cell viability was determined using the MTT assay. The
3 percentage of growth was calculated, with 100% representing control cells.
4
5 The results are the means \pm standard error from duplicate experiments.
6
7

8
9 B. Alternative splicing analysis of specific mRNAs. In five independent
10 experiments, SH-SY5Y cells were treated with 0.75 mM PQ for 18 h. Total
11 RNA was extracted, and the alternatively spliced regions of the indicated
12 mRNAs mRNAs were amplified by RT-PCR using primers that span the
13 alternative exons. After separation the PCR products were quantified as
14 described in Materials and methods. The bars show the average fold increase
15 of the indicated isoform after PQ treatment; error bars indicate the standard
16 error.
17
18
19
20
21
22
23

24
25 C. Agarose gel electrophoresis of *APAF1* and *BCL2L1* RT-PCR products.
26 Specific bands are labelled on the right of each panel. Marker: 100-bp ladder.
27
28
29
30
31
32
33
34
35
36
37
38
39
40
41
42
43
44
45
46
47
48
49
50
51
52
53
54
55
56
57
58
59
60

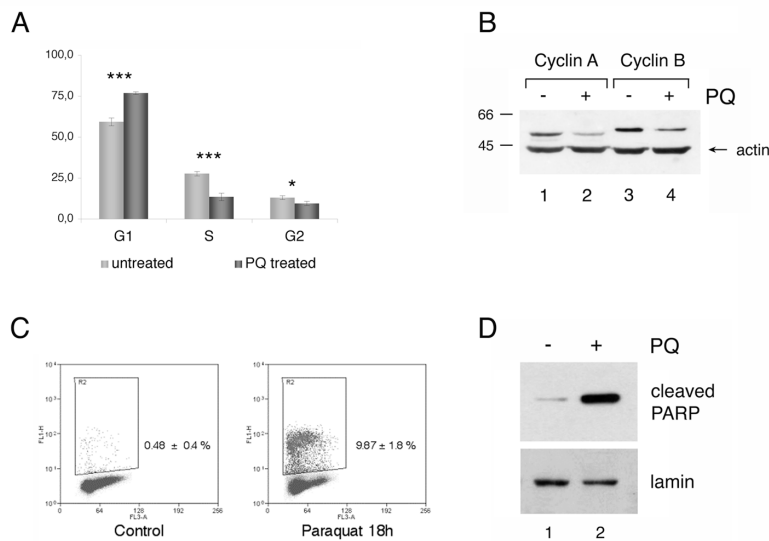


Figure S2

Figure S2. Experimental validation of the gene-level microarray data.

- A. Analysis of cell cycle phase distribution of SH-SY5Y cells after treatment with 750 μ M PQ. Quantifications were performed by flow cytometry after 18 h of treatment on cells stained with propidium iodide. Data are means of three independent experiments; error bars show standard errors. Bars identified by three asterisks have a p value ≤ 0.001 while those labelled with one asterisk have a p value = 0.01 to 0.05.
- B. Western blot analysis for cyclin A and cyclin B performed on whole cell extracts prepared from untreated SH-SY5Y cells and treated with 0,75 mM PQ for 18 h.
- C. Representative dot plots of untreated control cells and cells treated with 0,75 mM PQ for 18 h. Cells were stained by the fluorescence based TUNEL reaction and analysed by flow cytometry. The fluorescent cell populations in region 2 (R2) consist of apoptotic cells.

1
2
3 D. Western blot analysis for cleaved PARP performed on whole cell extracts
4 prepared from untreated SH-SY5Y cells and treated with 750 μ M PQ for 18 h.
5
6
7
8
9
10
11
12
13
14
15
16
17
18
19
20
21
22
23
24
25
26
27
28
29
30
31
32
33
34
35
36
37
38
39
40
41
42
43
44
45
46
47
48
49
50
51
52
53
54
55
56
57
58
59
60

For Peer Review

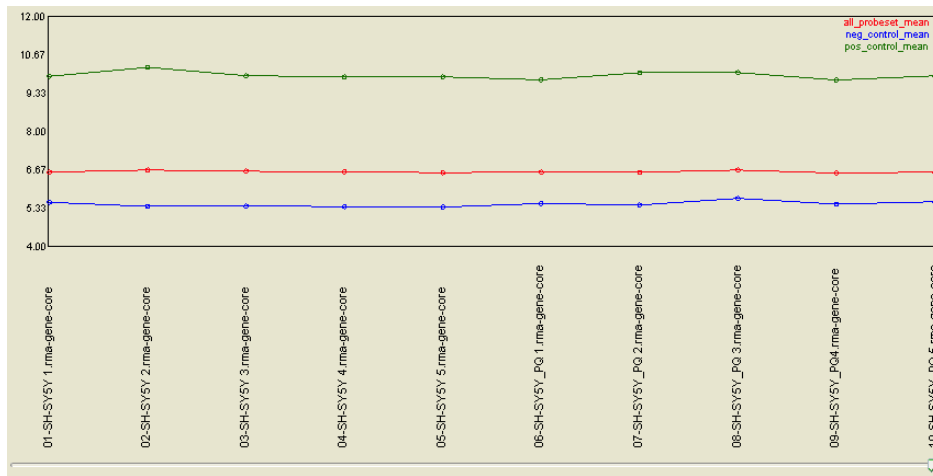


Figure S3. **All probe sets, negative and positive controls signal intensities in PQ-treated SH-SY5Y cells experiment**

“All probe set” quality control metric: red line. It represents the intensity signal of all the probe sets analyzed.

“Neg control” quality control metric: blue line. It represents the intensity signal of the set of putative intron-based probe sets from putative housekeeping genes.

“Pos control” quality control metric: green line. It represents the intensity signal of the set of putative exon based probe sets from putative housekeeping genes.

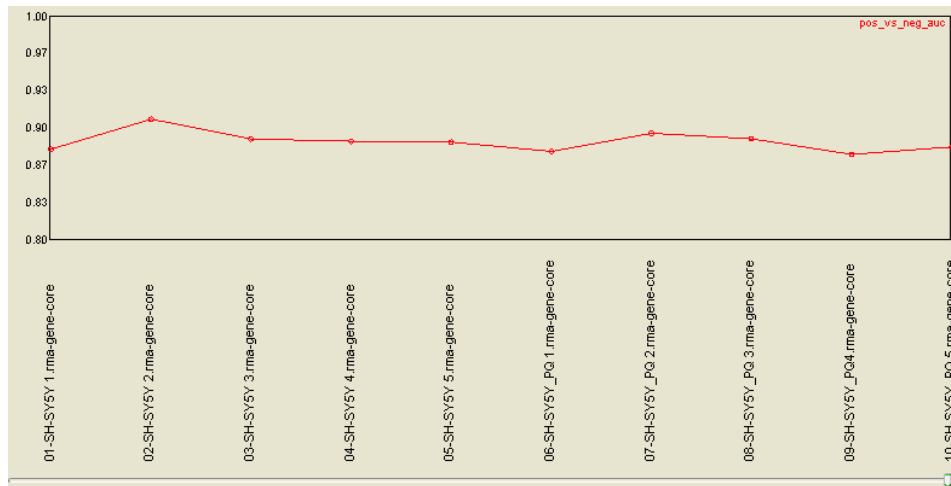


Figure S4. **Positive vs Negative auc line graph in PQ-treated SH-SY5Y cells experiment.**

Pos vs neg auc is the area under the curve (AUC) for a receiver operating characteristic (ROC) plot comparing signal values for the positive controls to the negative controls. The ROC curve is generated by evaluating how well the probe set signals separate the positive controls from the negative controls with the assumption that the negative controls are a measure of false positives and the positive controls are a measure of true positives. An AUC of 1 reflects perfect separation whereas as an AUC value of 0.5 would reflect no separation. In practice the expected value for this metric is tissue type specific and may be sensitive to the quality of the RNA sample. Values between 0.80 and 0.90 are typical.

“Pos vs neg auc” quality control metric: red line.

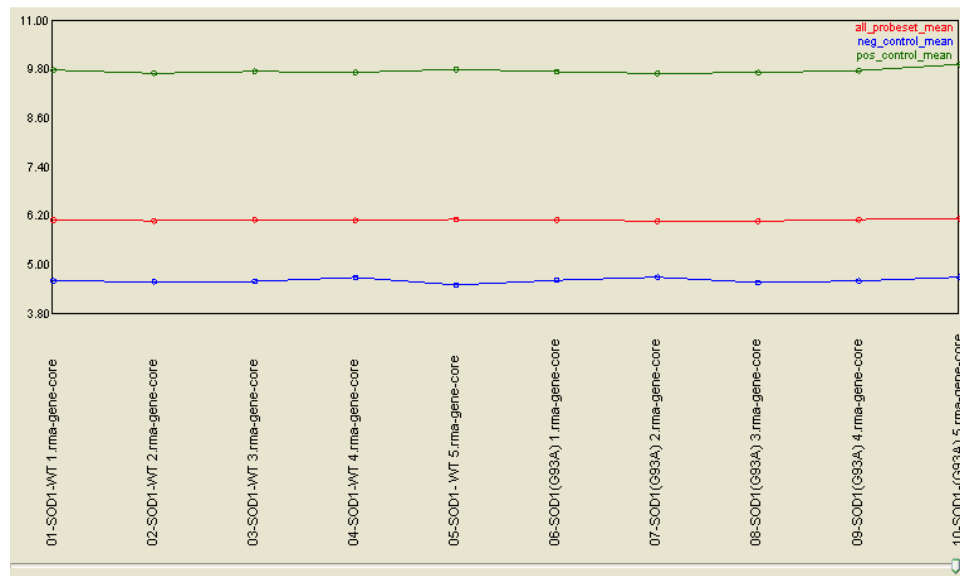


Figure S5. “All probe sets”, “negative “ and “positive” control signal intensities in experiment performed in SOD1 wt vs SOD1(G93A) SH-SY5Y cells.

“All probe set” quality control metric: red line. It represents the intensity signal of all the probe sets analyzed. The quality metrics reported for this category are going to be driven by the main source of content in that particular analysis. Thus the metrics reported for this category will be the most representative of the quality of the data being used downstream. For a good set of arrays, this intensity value does not have to vary.

“Neg control” quality control metric: blue line. Pos control” quality control metric: green line.

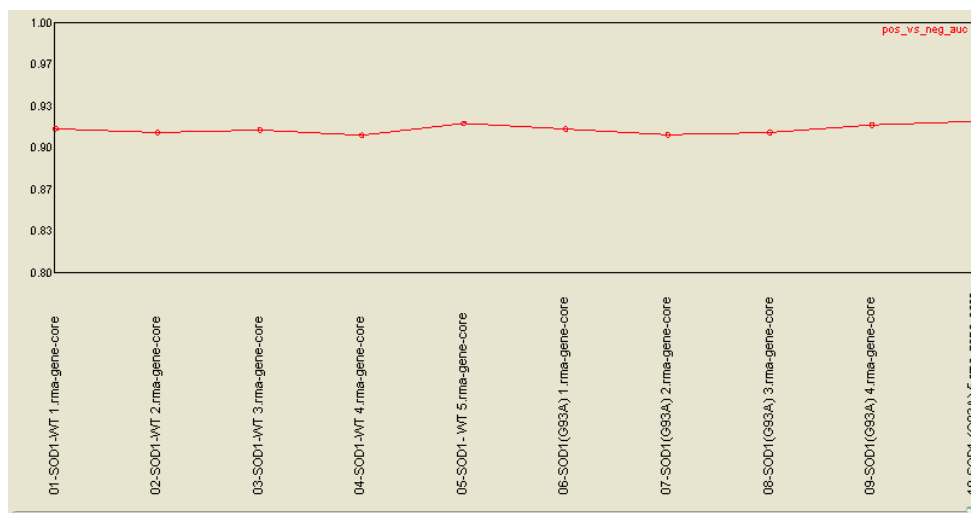


Figure S6. **Positive vs. Negative AUC line graph in the experiment performed in SOD1 wt vs SOD1(G93A) SH-SY5Y cells.**

“Pos vs neg auc” is the area under the curve (AUC) for a receiver operating characteristic (ROC) plot comparing signal values for the positive controls to the negative controls. The ROC curve is generated by evaluating how well the probe set signals separate the positive controls from the negative controls with the assumption that the negative controls are a measure of false positives and the positive controls are a measure of true positives. An AUC of 1 reflects perfect separation whereas as an AUC value of 0.5 would reflect no separation. Values between 0.80 and 0.90 are typical. “Pos vs neg auc” quality control metric: red line.

Deleted: ¶

¶
¶

-----Page Break-----

References¶

Birney E, Stamatoyannopoulos JA, Dutta A, Guigo R, Gingeras TR, Margulies EH, Weng Z, Snyder M, Dermitzakis ET, Thurman RE and others. 2007. Identification and analysis of functional elements in 1% of the human genome by the ENCODE pilot project. *Nature* 447(7146):799-816.¶
Castello PR, Drechsel DA, Patel M. 2007. Mitochondria are a major source of paraquat-induced reactive oxygen species production in the brain. *J Biol Chem* 282(19):14186-93.¶
Cicchetti F, Drouin-Ouellet J, Gross RE. 2009. Environmental toxins and Parkinson's disease: what have we learned from pesticide-induced animal models? *Trends Pharmacol Sci* 30(9):475-83.¶

¶

Supp. Table S6. Genes associated to Neurological Disorder, Axonal Guidance Signaling, and Neuritogenesis

Neurological Disorders

SYMBOL	DESCRIPTION
ADORA2A	adenosine A2a receptor
ADRBK2	adrenergic, beta, receptor kinase 2
AKR1B1	aldo-keto reductase family 1, member B1 (aldose reductase)
ASCL1	achaete-scute complex homolog 1 (Drosophila)
CACNG4	calcium channel, voltage-dependent, gamma subunit 4
CDON	Cdon homolog (mouse)
CHRM2	cholinergic receptor, muscarinic 2
CLU	clusterin
DHCR24	24-dehydrocholesterol reductase
GRM7	glutamate receptor, metabotropic 7
HSPA2	heat shock 70kDa protein 2
KIT	v-kit Hardy-Zuckerman 4 feline sarcoma viral oncogene homolog
LYN	v-yes-1 Yamaguchi sarcoma viral related oncogene homolog
MSH2	mutS homolog 2, colon cancer, nonpolyposis type 1 (E. coli)
MSRB2	methionine sulfoxide reductase B2
NDRG2	NDRG family member 2
NQO1	NAD(P)H dehydrogenase, quinone 1
NTRK1	neurotrophic tyrosine kinase, receptor, type 1
PREP	prolyl endopeptidase
SCG2	secretogranin II (chromogranin C)
SERPINE2	serpin peptidase inhibitor, clade E (nexin, plasminogen activator inhibitor type 1), member 2
SERPINI1	serpin peptidase inhibitor, clade I (neuroserpin), member 1
SMARCA2	SWI/SNF related, matrix associated, actin dependent regulator of chromatin, subfamily a, member 2
SPARCL1	SPARC-like 1 (hevin)
ST8SIA2	ST8 alpha-N-acetyl-neuraminide alpha-2,8-sialyltransferase 2
TIMP1	TIMP metalloproteinase inhibitor 1
TNFRSF1A	tumor necrosis factor receptor superfamily, member 1A
TUBB4	tubulin, beta 4

Axonal Guidance Signaling

SYMBOL	DESCRIPTION	paraquat Log2FC	SOD1 (G93A) Log2FC
BMP7	bone morphogenetic protein 7	-0.517	-2.050

1				
2				
3	DPYSL5	dihydropyrimidinase-like 5	-1,365	-0,529
4	EPHA6	EPH receptor A6	-0,702	-0,581
5	NTRK1	neurotrophic tyrosine kinase, receptor, type 1	-1,115	-0,749
6	PLXNA4	plexin A4	-0,684	-0,699
7	SDC2	syndecan 2	-0,908	-1,229
8	SEMA3D	sema domain, immunoglobulin domain (Ig), short basic domain, secreted, (semaphorin) 3D	0,999	1,136
9	SEMA6A	sema domain, transmembrane domain (TM), and cytoplasmic domain, (semaphorin) 6A	-1,131	-0,561
10				
11				
12				
13				

Glycerolipid Metabolism

SYMBOL	DESCRIPTION
AKR1B1	aldo-keto reductase family 1, member B1 (aldose reductase)
PPAP2B	phosphatidic acid phosphatase type 2B
GLB1L2	galactosidase, beta 1-like 2

Glycosphingolipid Biosynthesis

SYMBOL	DESCRIPTION
GLB1L2	galactosidase, beta 1-like 2
ST8SIA2	ST8 alpha-N-acetyl-neuraminide alpha-2,8-sialyltransferase 2

Genes related to neuritogenesis.

SYMBOL	DESCRIPTION	paraquat	SOD1 (G93A)
		Log2FC	Log2FC
FEZ1	fasciculation and elongation protein zeta 1 (zygin I)		-2.047
ISL1	ISL LIM homeobox 1	-1.208	
FOXD1	forkhead box D1		-1.373
FOXM1	forkhead box M1	-1.020	
FOXD4L3	forkhead box D4-like 3	0,955	0,895
LHX9	LIM homeobox 9	-1.881	1.685
LMO3	LIM domain only 3 (rhombotin-like 2)	-3.470	-3.598
LMO7	LIM domain 7	-0,553	-0,581
NEUROD1	neurogenic differentiation 1	-2.029	
NEUROG2	neurogenin 2	-2.631	

Supp. Table S8. Main Entrez Gene abbreviations used in the text

1
2
3
4
5
6
7
8
9
10
11
12
13
14
15
16
17
18
19
20
21
22
23
24
25
26
27
28
29
30
31
32
33
34
35
36
37
38
39
40
41
42
43
44
45
46
47
48
49

Gene Name	GeneID	Official Name
ABLIM1	3983	actin binding LIM protein 1
AKR1B1	231	aldo-keto reductase family 1, member B1 (aldose reductase)
ASCL1	429	achaete-scute complex homolog 1 (Drosophila)
ATF3	467	activating transcription factor 3
BIN1	274	bridging integrator 1
BTG2	7832	BTG family, member 2
CCNA2	890	cyclin A2
CCNB1	891	cyclin B1
CCNE2	9134	cyclin E2
CDKN1A	1026	cyclin-dependent kinase inhibitor 1A (p21, Cip1)
CDKN3	1033	cyclin-dependent kinase inhibitor 3
CHN1	1123	chimerin (chimaerin) 1
CXCR4	7852	chemokine (C-X-C motif) receptor 4
ERBB3	2065	v-erb-b2 erythroblastic leukemia viral oncogene homolog 3 (avian)
GADD45A	1647	growth arrest and DNA-damage-inducible, alpha
GLB1L2	89944	galactosidase, beta 1-like 2
GNAO1	14681	guanine nucleotide binding protein (G protein), alpha activating activity polypeptide 0
HGF	3082	hepatocyte growth factor (hepapoietin A; scatter factor)
KIF1A	547	kinesin family member 1A
LMO3	55885	LIM domain only 3 (rhombotin-like 2)
LRRK2	120892	leucine-rich repeat kinase 2
MDM2	4193	Mdm2 p53 binding protein homolog (mouse)
NEUROG3	50674	neurogenin 3
NTRK1	4914	neurotrophic tyrosine kinase, receptor, type 1
NKX2.2	4821	NK2 homeobox 2
NRG1	3084	neuregulin 1
PARK7	11315	Parkinson disease (autosomal recessive, early onset) 7
PAX6	607108	paired box 6
PINK1	65018	PTEN induced putative kinase 1

1			
2			
3	PLXNA4	91584	plexin A4
4	POLH	5429	polymerase (DNA directed), eta
5	PPAP2B	8613	phosphatidic acid phosphatase type 2B
6	PPM1D	8493	protein phosphatase 1D magnesium-dependent, delta isoform
7	RPRD1A	55197	regulation of nuclear pre-mRNA domain containing 1A
8	SDC2	6383	syndecan 2
9	SEMA3A	10371	sema domain, immunoglobulin domain (Ig), short basic domain, secreted, 10 (semaphorin) 3A
11			
12	SESN1	27244	sestrin 1
13	SESN2	83667	sestrin 2
14	ST8SIA2	8128	ST8 alpha-N-acetyl-neuraminide alpha-2,8-sialyltransferase 2
15	TP53INP1	94241	tumor protein p53 inducible nuclear protein 1
16	VSNL1	7447	visinin-like 1
17	WASF3	10810	WAS protein family, member 3
18			
19			
20			
21			
22			
23			
24			
25			
26			
27			
28			
29			
30			
31			
32			
33			
34			
35			
36			
37			
38			
39			
40			
41			
42			
43			
44			
45			
46			
47			
48			
49			

1
2
3
4
5
6
7
8
9
10
11
12
13
14
15
16
17
18
19
20
21
22
23
24
25
26
27
28
29
30
31
32
33
34
35
36
37
38
39
40
41
42
43
44
45
46
47
48
49

Supp. Table S9. Oligonucleotide primers

Nucleotide sequences of the primers employed for RT-PCR real time

Species: Homo sapiens

Gene ID	Forward_Sequence (5'-3')	Reverse_Sequence (5'-3')	Product length (nt)
ADAMTs1	TTTGATAAATGTGGTGTTCGCG	TTTTGCACTAGTAACTGATCCTG	75
AIFM2	CGTCAACTCTGTGAAGCA	CATGGACAGGAGGAACG	70
APBA1	CACGAGAAGATCGTCCAC	GGCTGGCATTGTCTTCA	66
ASCL1	GACTTTGGAAGCAGGGT	CAACGCCACTGACAAGAA	62
CABLES1	GGGTGCTGATGGGAAGACT	CAGGTTACGGAACGGGAGA	115
CHN1	GTATGTAGGCATCTTTCATTTCAGA	CAAAACACTCAGCATCTCTCTTT	129
CNTN4	CTGTCAGCCATCAGTACAATAAT	AGCAAGTCCTTCAGATAACTTT	78
CXCR4	ATTGGGATCAGCATCGACTC	CAAACCTCACACCCTTGCTTG	61
EPHA6	AAGGAGATTGATCCCTCAAGAA	CGCCCACTACAGACTTCTCC	77
GAPDH	ACGGATTGGTCGTATTGGG	TGATTTTGGAGGGATCTCGC	231
GPM6B	CCTGGAGAACATCTGCAAC	GGCCACAATGAACAGGT	61
HGF	AGCATGTCTCCTGCATCTC	TTGTATTTCTTCTTTTCCTTTGTCC	78
ITGA9	TGCTCTGGAAGATGGGC	GGTTCCTCTCAGCTTCGATAATTT	63
LMO3	CTTTGCATGTCAGCTTTGTAAT	CCTTCCTCGTAGTCCGT	96
NRP2	GGACCCCAACTTGGATT	ATGGTTAAAAAGCGCAGGTC	61
NTRK1	GAGGCAATCGACTGCATCA	GTAGACCTCTGGTGGGC	69
NUDT11	TTCGGTTAGCATTGGGAGG	GCTTGTGGCACTGGAGAA	74
SDC2	GTCCTAGCAGCTGTCATT	TACACCAACAGCAGGATAAGAAA	74
SEMA3A	GCGAAATGAAGAGCGAAAAG	TTTGTATGAACCCATGTTCCAC	140
SLIT3	CTTGTCTCCCTGTCCACCATA	CCTCTTCCTCAACCACTTGC	90
SLITRK6	TACGCAGTGGTTGGTGTTC	TCCACAGCTTCATGTTGTCAT	146
SMARCA2	AAACCTGTAGTGAGCGATT	TCATCATCCGTCCCACTT	80
TNIK	AGCTCAAAGGTTAAAGTTTCTATG	TTCCTCCAGATCGCAGC	71

VSNL1	GTGATGGCAAGATCACCC	ATCACAGTGCCTACCATT	73
WASF3	CGAATGGGAATTCAACTGAAA	GTCATTCCCCACTGGCT	75
ZNF521	GCAGAATCATAACAATGACCCA	AATCAATTCTCCTTGAGAGACT	65

For Peer Review

Species: *Mus musculus*

Gene ID	Forward_ Sequence (5'-3')	Reverse_Sequence (5'-3')	Product lenght (nt)
Cdc42	ACAACAAACAAATTCCTATCG	TTGCCCTGCAGTATCAAAAA	114
Cxcr4	TGGAACCGATCAGTGTGAGT	GGGCAGGAAGATCCTATTGA	131
Fez1	AAGGCATCTCCAACATCCTG	AGCATCTGCAGGTCTTCCAC	136
Hgf	CACCCCTTGGGAGTATTGTG	GGGACATCAGTCTCATTACAG	66
Hprt1	TCCTCCTCAGACCGCTTTT	CCTGGTTCATCATCGTAATC	90
Nrp2	CGAAGTGAGAAGCCAGCAA	GAGGGATAGTCCTGGGGGTA	99
Ntrk1	GGACCTCAACCGTTTCCTC	CCATACCAGCAGCCACCT	131
Sema3a	GGGAAGAGCCCTTATGATCC	CCGCAGCAGTTCAGAGTA	79
Sept2	CAGTGAAGAAGGGTTCGAG	TCTGGGTAGAGATCAGTCAGGA	103
Sept7	AGGGGATGTCGGTCAGTG	CAAGGTTCTTCGGTTGAGCTA	87
Slit1	AACGTGGCAGAGGTGCAA	GCAGGAACCGGACGAGAG	93
Slit2	CTGTCATGGGCTGGCACT	TCCTCGTGATGTTATTTCCATTC	89
Slit3	ACCGGTTCCAGTGCAAAG	TGCAAGTGCCGTTGTTCTT	93
Wasf3	CTGTGGCTGAGGCCAAAGC	TGCACCTTTTTTCAGTTGGATT	106

Figures for Referee 2

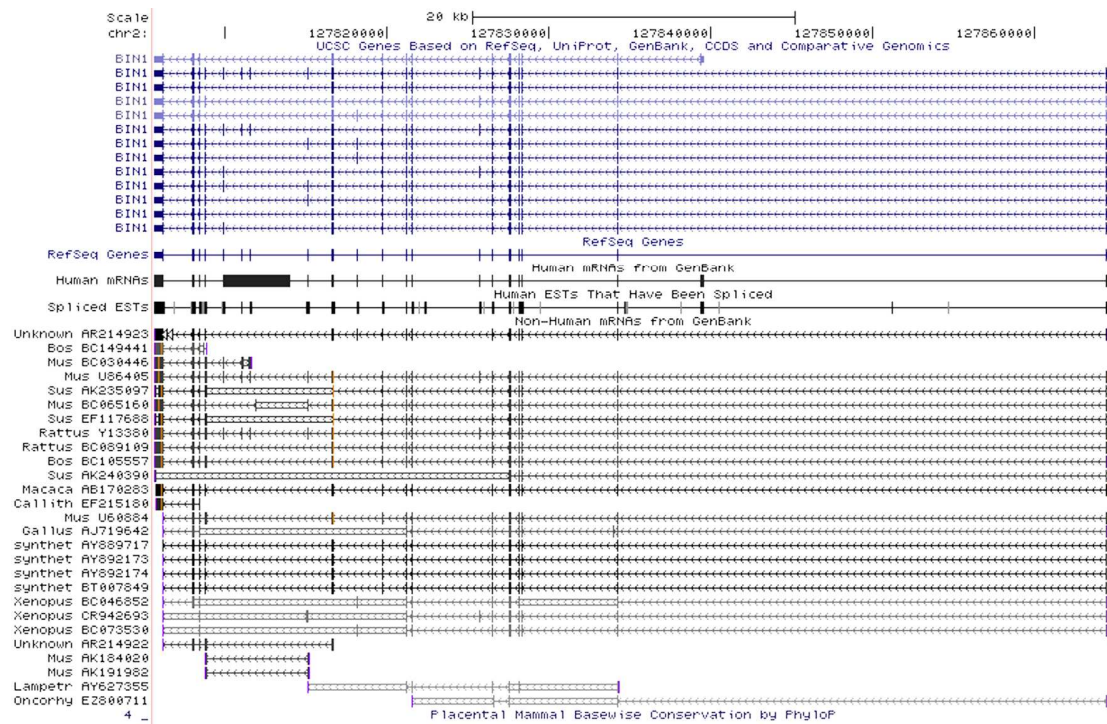


Figure R1. Comparison of the human and mouse *BIN1* gene structure (UCSC Genome Browser).

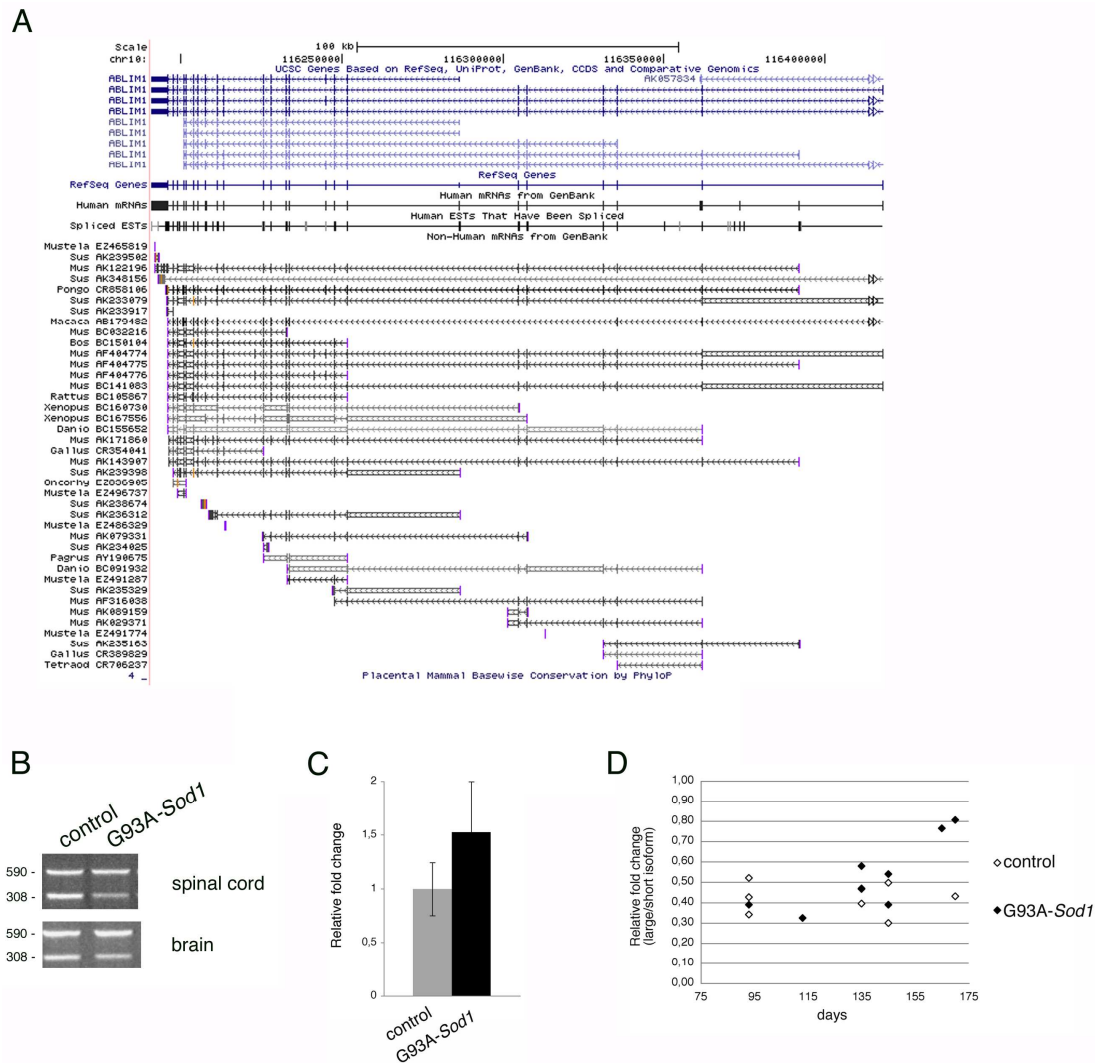


Figure R2

Figure R2. Analysis of the alternative first exon usage in the G93A-Sod1 mouse.

- Comparison of the human and mouse *ABLIM1* gene structure (UCSC Genome Browser).
- RT-PCR analysis of the transcripts including the two putative first exons.
- Quantitation of the PCR fragments. The bar graph represents the quantitation of the RT-PCR analysis for the long and the short *Ablim1* mRNA variants. The first exon switch was normalized relative to that observed in the respective control (light grey bars). The dark grey bars show the average fold-change of the short mRNA variant transcribed from proximal promoter; error bars indicate the standard error.
- Time course analysis of long *Ablim* transcript in the spinal cord of G93A-Sod1 mice during disease progression. Plotted is the ration of the long over the short mRNA variant normalized to that of age-matched non-transgenic control animals (opened circles) on different days from the pre-onset till the symptomatic stage (93-170 days).